Analysis of a major Aeolian dust input event and its impact on element fluxes and inventories at the DYFAMED site (Northwestern Mediterranean)

José Luis Mas[1*], Jacobo Martín[2], Mai Khanh Pham[3], Elena Chamizo[4], Juan-Carlos Miquel[3], Iolanda Osvath[3], Pavel P. Povinec[5], Mats Eriksson[6,7], María Villa Alfageme[8]

[1]Dpto. Física Aplicada I, ETSII, Universidad de Sevilla, 41012 Sevilla, Spain.
[2]CADIC-CONICET, Bernardo Houssay 200. Ushuaia, 9410, Argentina.
[3]IAEA-Environment Laboratories, Monte Carlo, 98000, Monaco
[4]Centro Nacional de Aceleradores (Universidad de Sevilla, Consejo Superior de Investigaciones Científicas, Junta de Andalucía). Thomas Alva Edison 7, 41092, Seville, Spain.
[5]Faculty of Mathematics, Physics and Informatics, Comenius University, SK-84248 Bratislava, Slovakia
[6]Swedish Radiation Safety Authority, Solna strandväg 96, 171 54 Solna, Sweden
[7]Linköping University, Division of Radiological Sciences, IMH, 581 83 Linköping, Sweden
[8]Dpto. Física Aplicada II, ETSIE, Universidad de Sevilla, 41012 Sevilla, Spain.
*E-mail address: ppmasb@us.es

Abstract

Continental dust can be suspended and transported by the wind, reaching seawater masses far away from its source. The deposition of the aerosols on the ocean surface can alter the abundance of chemical species in the water column and contribute to element inventories in seafloor sediments. A major Saharan dust intrusion into the Western Mediterranean Sea was recorded at the DYFAMED site (Ligurian Sea) in 20th February 2004. We determine the influence of this dust event on the concentration of 30 major and trace level elements (TE) in sinking particles collected by sediment traps deployed at 200 m and 1000 m depth, and how a dust flux event like this contribute to the exchange of TE, including Fe, with the water column during major dust events. With coupled sediment traps and aerosol samples, we assessed the short-term implications of dust events in the water column. The event produced a flux of fast (> 111 m d^{-1}) and slow (< 20 m d^{-1}) sinking dust particles, detected during 3 weeks at 200 m and 4 weeks at 1000 m depth. This study demonstrates that a single dust deposition event can produce a sinking flux equivalent to annual deposition rates of elements relevant to biogeochemical cycles and/or pollution studies: (>60% for Cr and Cu, >70% for Al, >80% for Ni and Zn, >90% for V and Mn, >100% for Fe and Pb). The corresponding Enrichment Factors (EF) in the sediment traps during the atmospheric dust as reference were calculated, which in the TE analysed in the traps ranged between 0.35 and 421 in both 200 m and 1000 m sediment traps. For most of the TE, EF >1. A few exceptions were V, Y, Zr, Nb, and Ce (EF ~ 1) and Cr, Ni, Cu, Zn,

Sn, and Pb (EF<1). Despite the variability in the EF values, vertical fluxes integrated during the dust event increased from 200 m to 1000 m, except for I, which decreased. This contrasts strongly with the element fluxes integrated for the complete sampling season, which decrease or increase from 200 m to 1000 m, depending on the element. This suggests that sinking dust particles are acting generally as sinks of the TE. We conclude that, apart from I, a substantial portion of the atmospheric dust input from one of these deposition events can reach the mesopelagic layer of the Western Mediterranean basin without increasing the budget of the dissolved TE.

1. Introduction

Measurements of trace element (TE) abundances and fluxes in the ocean can contribute to our understanding of biogeochemical processes, which can influence global climate (Baskaran, 2011; Schlitzer et al., 2018). Ocean time series studies are one way in which we have increased our knowledge about the cycling of TE and their fluxes across the atmosphere, ocean, and seafloor boundaries (e.g. Karl and Lukas, 1996; Steinberg et al., 2001).

The DYFAMED (Dynamique des Flux Atmospheriques en MEDiterranee) sampling station in the Northwestern Mediterranean Sea (Figure 1) was established in 1988 as a part of the international efforts to better understand ocean biogeochemical cycles and the nature of air, land and sea exchanges (Buat-Menard and Lambert, 1993; Miquel et al., 2011). One DYFAMED sampling activity is an instrumented mooring line, equipped with sediment traps at nominal depths of 200 m and 1000 m. The site is located ~ 50 km off the coast of Monaco, over a total water depth of 2350 m. While considered an open ocean station, it is influenced by aeolian inputs and, under certain conditions by continental/riverine inputs (e.g. Ternon et al., 2010). Sporadic intrusions of dust from northern Africa are known to affect this region primarily during spring and summer, supplying an important lithogenic flux that could perturb TE budgets within the water column and the sediments (Ternon et al., 2010; Scheuvens et al., 2013; Marconi et al., 2014). Its proximity to densely populated areas with urban and industrial activities cannot be disregarded either (Guerzoni et al., 1999; Béthoux et al., 2002). The time-series site's proximity to land-based pollution influences the sea surface through the transfer of continental aerosol to the open sea and is ultimately stored in the sedimentary record through the downward flux of particulate matter and by lateral transport along the Var Canyon system (Migeon et al., 2006; Martín et al., 2009).

The contribution of lithogenic fluxes from Saharan dust to particle export in the Northwestern

Mediterranean Sea has been already analyzed in the context of studies on the biological carbon pump (Ternon et al., 2010; Miquel et al., 2011; Heimbürger et al., 2013; Jones et al., 2013; Pasqueron de Fommervault et al., 2015). However, the role of heavy Saharan dust deposition events on the inventories of TE water column and sediments has not been characterized in detail (Migon et al., 1997, 2002; Heimbürger et al., 2014).

During February 2004, a major Saharan dust deposition event was observed in the Northwestern Mediterranean,. A dust deposition flux of 19.8 g m^{-2} d^{-1} was measured on February 20th at Monaco (Pham et al., 2017), and detected within few days in sinking particles collected by sediment traps at 200 m and 1000 m depth at the offshore DYFAMED site (Ternon et al., 2010; Miquel et al., 2011). A study by Pham et al. (2017) described the impact of this event on the vertical fluxes of natural and artificial radionuclides. This work concluded that for many of the analyzed radioisotopes, this single dust deposition event was able to supply most of the annual flux. This suggested that the vertical fluxes and inventories in the water columns of other TE could be impacted in a similar way. To the best of our knowledge, multi-element analyses of these major dust deposition events have not been published yet.

This paper provides new information on the geochemical impact of massive dust deposition events and addresses the following topics: i) the fate of the atmospheric input based on geochemical tracers in the water column; ii) how events of this type can affect the abundance of TE, especially if they provide a significant input of dissolved nutrients, lithogenic and particle-reactive elements; iii) if these dust events act as net sources via dissolution or net sinks via scavenging of TE in the water column.

2. Materials and methods

Sinking particles were collected at the DYFAMED site (43º25’ N, 7º52’ E; Figure 1) using PPS3/3 Technicap sediment traps (Heussner et al., 1990) attached to a mooring line at 200 m and 1000 m. During the period of this study (December 2003 to May 2004), the sampling interval of the sediment traps was 14 days, with only one deviation from that schedule: the rotary mechanism of the 200 m-depth traps failed in the ninth sample, thus the last bottle integrates 4 sampling intervals (56 days). A complete description of the mooring lines and details of sediment trap sample processing can be found in Miquel et al. (2011).

Atmospheric dust was collected using a 2×2 m^2 stainless steel funnel-type collector located on the roof of the IAEA-EL (International Atomic Energy Agency- Environmental Laboratories) premises in Monaco (43º45'N, 07º25'E), using the methodology described in Pham et al. (2003, 2017). The IAEA-EL sampling site is located on the coast, 70 m above sea level and 52 km from the DYFAMED site. Element concentrations of both sample's types were determined by X- ray fluorescence (Spectro X-Lab 2000) (Martín et al., 2009). Briefly, aliquots of 1-4 g of dried and ground solid sample were analyzed in calibrated XRF cups covered with Prolene® thin film. Analyzes for the elements Al to U were done by using a combination of three measurements with different X-ray targets. Analytical uncertainties for the elements considered in this study were always below 5%. When required, exploratory statistical analyses were performed using Statgraphics Centurion XVI.

The Enrichment Factor (EF) is defined here as the factor by which the concentration of a given TE in sinking particles is greater or lower than its average concentration in the Earth's crust or in a sample from a specific region, like the Saharan desert. In this study, the EF was used to determine the enrichment of TE in sinking particles and as a proxy for the origin of collected particles.

TE concentrations were normalized to the concentration of Al, an abundant species in soil and dust samples.

Thus, the enrichment factor (EF) is calculated as follows,

$$EF = \frac{[M]_{sample} / [Al]_{sample}}{[M]_{SD-1} / [Al]_{SD-1}} \quad (1)$$

where M_{sample} and Al_{sample} are the concentrations of the element M and Al respectively, measured in the particles collected in the traps. M_{SD-1} and Al_{SD-1} are the concentrations of the element M and Al in the SD-1 aerosol samples collected in Monaco. EF describes the enrichment or depletion of TE in relative to dust sample.

The use of vertical fluxes provides complementary information to that of EF values. Vertically integrated fluxes are calculated for the different TE as

$$\Phi_{TM} = \sum_i c_{iM} \Phi_{miM} \Delta t_i \quad (2)$$

where the Φ_{TM} is the integrated vertical flux (mg/m^2 or µg/m^2) for the element M, the c_{iM} (mg/g,

μg/g) is the concentration found for the element M in the sediment trap samples collected during the i-th sampling interval, the Φ_{miM} is the mass flux (g/m^2 d) collected for such sampling interval, and Δt_i (d) is the length of the i-th sampling interval. Uncertainties were calculated using normal propagation of errors; in this way it is possible to find relative uncertainties of the total vertical flux lower than the relative uncertainty of the i-th vertical flux.

3. Results and discussion

3.1. Main characteristics of the Saharan dust intrusion event

Two dust deposition events were detected at the IAEA-EL aerosol station during the study period (Table 1). Previous studies have attributed these events to suspension of Saharan desert dust (Libya/Algeria) (Scheuvens et al., 2013). The relationships between concentrations of major elements and trace radionuclides in the collected aerosols confirm such origin (Pham et al., 2017). The first event was observed during 20th-21st February 2004 (but called in whole text as 20th February 2004, for short). A second, less intense, dust deposition event was detected during 1st-2nd May 2004 (Pham et al., 2017). These two events of Saharan dust deposition will be hereafter abbreviated as SD-1 and SD-2 respectively, however we will focus mainly on the analysis of SD-1 which has much more intense deposition than SD-2.

Tables 2a and 2b display the correlations of the concentrations of the TE in the context of the Saharan dust. At 200 m depth, highly significant positive correlations were found for certain groups of elements. This includes 1) major/trace elements associated with the mineral component of the dust particles (Al, K, Ti, Fe, Y), 2) major nutrients associated with biological cycling (P, S, Br, I), and 3) intermediate trace elements including important contributors to the hard parts of biota and biologically-essential micronutrients (Ca, Ni, As, Sr, Mn). It is worth noting that when the 1000 m-depth data were analyzed, good correlation between phosphorus and iodine found at 200 m depth disappears (0.7405, $p < 0.05$; Table 2.b). However, for the rest of the elements the correlations remain significant.

The TE concentrations of the dust particles collected in Monaco are in agreement with Saharan soil concentrations (Gross et al., 2016; Marconi et al., 2014; Scheuvens et al., 2013, Tables i.a-i.d [Supplementary material]). This corroborates the results of previous works that used long-lived radioisotopes (e.g., ^{238}U) as tracers of lithogenic particles during the SD-1 and SD-2 events (Pham et al., 2017).

As noted by Miquel et al. (2011), the effect of the SD-1 deposition event on particle fluxes in the DYFAMED sediment traps was fast and remarkable, resulting in the highest mass flux collected by the DYFAMED sediment traps up to that date. The sinking flux collected during SD-1 was an order of magnitude higher than the mean annual flux, at both 200 m and 1000 m depth (Miquel et al., 2011), and almost one order of magnitude higher than other dust deposition events at DYFAMED (e.g. May 2005, July 2005 or May 2008; Pham et al., 2017).

The timing of SD-1 (late winter) coincided with the seasonal overturning of the water column in the study area, which may have facilitated the deep export of sinking particles. During late winter, the hydrographic conditions in the open Northwestern Mediterranean are characterized by strong convection following surface cooling (e.g. Martin et al., 2010); as a consequence, there is an intense vertical export of both dissolved and particulate material centered around February (Migon et al., 2002; Heimbürger et al., 2014). In addition to this physical mechanism, phytoplankton blooms occur following the convection period and the sinking of biomass contributes to the downward flux of minerals by scavenging and aggregation (Ternon et al., 2010; Miquel et al., 2011).

We divided the sampling period into different phases based on particles flux (Figure 2a and Table 1). There is a first stage from December 2003 to February 2004, before the dust event. In the first phase (Dec 2003-Feb 2004, prior to SD-1), total mass fluxes ranged 42 – 176 mg m^{-2} d^{-1} at 200 m and 85 – 151 mg m^{-2} d^{-1} at 1000 m-depth, typical fluxes for the season at the site (Miquel et al., 2011). The sinking particles collected in the traps were a complex mixture of organic matter, biogenic silica and particulate inorganic material (calcite and lithogenic components) (Miquel et al., 2011; Ternon et al., 2010). This heterogeneous material, generally defined as “marine snow” (Le Moigne et al., 2013; Villa Alfageme et al., 2014) can accumulate TE through adsorption, aggregation, or bioaccumulation. Particle sinking velocities and the temporal evolution of enrichment factors and element flux values before the dust event are related to these mechanisms.

The sinking mass flux at 200m abruptly increased (sediment trap sample ST6, see Table 1) by more than an order of magnitude, up to 1200 mg m^{-2} d^{-1} ., in concordance with the occurrence of the SD-1 event.

Most of the particles collected from 15th February to 28th March (ST6, ST7 and ST8) at a depth of 200 m correspond to atmospheric dust particles from the Aeolian event. SD-1 was detected at the 1000 m sediment trap samples corresponding to 15th February-11th April (ST6, ST7, ST8 and ST9).

During the stage of the dust event SD-1 following 28th March 2004, the particle flux decreased to approximately pre-dust event values, down to 200 mg m^{-2} d^{-1} at a depth of 200 m. Another increase in the particle mass flux, centered around May 2004, was possibly associated with event SD-2, . This secondary increase was clearly seen at 1000 m depth, but not at 200 m depth. This can be partly due to the fact that at 200 m, the sample that includes the dust collection of that week integrates over two months of sampling, instead of 15 days. Also, deposition of slow-settling particles can account for a delayed arrival of the downward flux (caused by SD-1) from 200 to 1000 m depth.

The velocity of the sinking dust particles was calculated based on the analysis of the above-described evolution of the mass fluxes along the season. The reference time used for both 200 m and 1000 m were the time elapsed between the detection of the atmospheric dust event in the IAEA-EL aerosol station (20/02/04) and the first detection of the dust particles by the sediment traps at 200 m (24/02/04) and 1000 m (24/02/04). Note that the moment of detection of the dust event by the traps correspond to the sediment trap ST6 that collected particles from 15/02/04 to 29/02/04, when particle flux increased one order of magnitude. However, we cannot be sure in which day during the two weeks of sampling the traps collected the first signal. For this reason, the moment of detection for ST6 was chosen as 24/02/2004, corresponding to the midpoint during the 2-week collection period. Using the earliest estimated date of the detection of the input, we obtained the maximum sinking velocities. We calculated that the velocity for fast particles at 1000 m was between 50 m d^{-1}, if the first pulse was detected on the 29/02/04, and 250 m d^{-1} if the first pulse was detected on the 24/02/04. The velocity of slow-sinking particles was estimated following the same approach. To estimate the reference time for the slow particles at 200 m, we selected the last day of ST8 (28/03/04) as a reference of the maximum flux observed at the last day of the dust event. Similarly, we selected the last day of ST9 (11/04/04) as the last day of the dust event detected at 1000 m. Using this data at 1000 m, we obtained a velocity of >20 m d^{-1} for the slow-sinking component of the flux.

To summarize, we estimated the sinking velocity of SD-1 dust particles to be > 20 m d^{-1} for slow-sinking particles and < 250 m d^{-1} for fast-sinking particles. These values are in the range of the values expected according to the density and size of collected material (Villa-Alfageme et al., 2016). Also, the sinking velocities of dust particles are in agreement and in the same order of magnitude as the sinking velocities of less dense biogenic sinking particles (Villa-Alfageme et al.,

2014).

3.2. Temporal evolution of dust impacts in the water column

Saharan dust is known to introduce zircon in the Mediterranean Sea, and the ratios of Zr/Al have been used as indicators of Saharan dust deposition events (Moreno et al., 2005). Figure 3 shows that this ratio increases notably and simultaneously at both sampling depths after the SD-1 event. After approximately two months, the element ratio returns to values similar to those previous to the SD-1 event.

Studying the evolution of EF and element flux parameters in the three dust event stages (prior to, during and at the dust events) described is key in understanding how dust events contribute to the exchange of TE in the water column.

3.2.1. Enrichment factors

The EF was used to analyze the evolution of the TE concentration in relation to the expected concentration in dust particles (Figures 2b-2e and in Tables 3a-3d). As described above, the sediment traps mainly collected dust particles between the period of 15 February to 28 March. Thus, according to this definition of EF, TE with an EF value of ~ 1 implies that there is not significant loss, or scavenging, of the TE from the sinking dust particle, i.e. there is no contribution of the element to the budget of the water column. When EF > 1, the sinking dust particles are removing TE dissolved in the water column while they sink, increasing the initial TE concentration of dust particles. Elements with EF < 1 imply that the dust particles have released part of the TE to seawater, i.e., there is a net contribution of the TE from the dust particles to the water. EF values of TE in particles collected in phase I, prior to SD-1, can be used as a baseline for our temporal analysis (Miquel et al., 2011).

Finally, we can compare EF values of TE at 200 m and at 1000 m to determine if the sinking particles changed their TE composition significantly from the euphotic zone to the mesopelagic.

An important remark about the uncertainties of the measurements and the interpretation of our conclusion is that our sediment traps are not Lagrangian traps and may therefore be affected by advective processes. Furthermore, the results were obtained from a single deployment and a unique sediment trap. This implies that the uncertainties associated with advection and local variability in the concentration of elements should be taken into account in our estimations.

Therefore, uncertainties associated with our measurements are higher than the statistical and instrumental uncertainties associated solely with the measurement.

3.2.2. Element integrated vertical fluxes

Figures 4a-4b show the temporal evolution of 4 element fluxes (S, Ca, Ti and Fe) integrated in the two-week period of the rotation of the traps at 200 m and 1000 m (See Supplementary Material, Part 2 for all elements). As a rule, all TE fluxes increase as the dust event starts and decrease when the event stops. This pattern may be due to the increase in total particle flux or may indicate an enhancement of TE in the particles. When combined with enrichment factors, we will attempt to distinguish these processes.

A decrease in the integrated element flux, from 200 m to 1000 m during SD-1, points to a release of the TE from the dust particles to the water column, probably due to remineralization of the sinking particles (Tables 4a and 4b). If the integrated element flux increases from 200 m to 1000 m, this is an indicator of net removal of TE from the water column while the particles sink. If the dust period integrated element flux remains constant at 200 m and 1000 m, this implies that there is no net transfer of TE from/to the water column, i.e., the dust particles do not contribute to the inventory of TE in the water column.

A similar comparison (i.e., 200 m *vs* 1000 m-depth) could be done for the whole sampling season. Note that the sampling season that we are considering for comparison to the dust event do not cover a whole year. That means that it is only a partial representation of particles fluxes along the year. Furthermore, the inclusion of results from the dust event in the whole sampling average might also influence the results of the complete sampling. Therefore, the results of the complete sampling months cannot be used to infer behaviors of TE for the whole year.

The general correlations of fluxes and EF in shallow and deeper depths are compared during the complete sampling and the dust event with the specific objective of examine if the changes in fluxes and EF in depth are constant for those months or it varies during the dust event. A clear difference in terms of TE fluxes and EF would indicate that the sinking particles behaves different during the dust event in relation to the contribution of TE to the water column budget.

3.2.3. *Enrichment factors (EFs) and element fluxes in most abundant TE*

The biogeochemical behavior of the most abundant TE in the sinking particles, Si, Ti, S, Fe and Ca before, during and after the dust event were analyzed (Tables 3a-3d and Figure 2b). The dust intrusion in the ocean was estimated to occur during 2-week period from 15 February to 29 February (sample ST6), when particle flux in the 200 m sediment traps increased by an order of magnitude. This intrusion can be confirmed by changes in the EF, which increased for Si and Ti and decreased for Ca. Within uncertainty, no changes were detected for Fe and S. During the dust event, the EFs for most abundant TE are higher than 1, which suggests that the dust particles are removing TE (relative to Al) from the water column while sinking in the first 200 m of the water column. It is important to emphasize that the uncertainties associated with these results are only instrumental and statistical. The elements are classified according to their EF values, but for the elements with higher concentrations, this classification is only a first approximation, and further measurements should be done to minimize these uncertainties. If the uncertainties given in Tables 3a-3d are considered, a conservative approach implies that only EF>1.5 values account for local variability.

We conclude that the classification is statistically robust only for S and Ca (EF>1.5), whereas Si, Ti and Fe have EF values < 1.5. If the uncertainty due to advection was included, we may not be able to classify the category with a better precision.

The evolution in EF values are qualitatively the same for these elements at both sampling depths, 200 m and 1000 m. Furthermore, EF values are very similar at both depths during the dust event. This implies that there is no significant change in the dust particles while sinking from 200 m to 1000 m and EFs remain approximately > 1, with no significant increase. The only exception is S, for which the EF in the last sample at 200 m depth is more than twice that at 1000 m depth. The element vertical fluxes displayed in Figures 4a-4b and Tables i.a-i.d (Supplementary material), show similar trends for Si, Ti, S, Fe and Ca at 200 m and 1000 m, with an expected significant increase of fluxes when the dust event starts (Si is not shown in the figures). This increase of the TE fluxes in the fortnight of 15th February (sample ST6) confirms that the SD-1 event started at that time.

When fluxes are integrated for the whole season (Tables 4a-4b), the flux from 200 m to 1000 m decreases very little (2% for Ca, ~ 5% for Si, Ti and Fe). The decrease with depth is only statistically significant for S (11%). The decrease in the TE fluxes at 1000 m over the whole season, except the dust period, may indicate that the sinking dust particles are being remineralized above 1000 m, and releasing dissolved TE into the water column.

Contrary to the entire seasonal estimates, the total element vertical fluxes at 200 m and 1000 m integrated exclusively for the dust period show an increase with depth. The increase is approximately 15% for Si, Ti, S, Fe and Ca (Tables 4a-4b). It can therefore be inferred that there was a net removal of major TE scavenged by the dust sinking particles from the water column during the dust event.

Among the most abundant TE, Fe is particularly significant because it is associated with mineral components of the dusts and plays an important role in the ocean biogeochemical cycles as a micronutrient. As described above, the EF results and the increasing total element fluxes from 200 m to 1000 m suggest that dust particles may remove Fe from the water column while sinking, and release Fe to the mesopelagic zone during remineralization. This dust event likely did not contribute to increasing the abundance of Fe, however unaccounted local variations in concentrations do not allow to completely validate this hypothesis.

Summarizing the results during the dust period for the most abundant TE, we conclude from the combination of the information provided by the EFs and the total integrated element fluxes that dust particles are not significantly transferring the major elements Si, Ca. Ti, and Fe to the water column. Indeed, dust particles seem to act as a sink for this set of elements.

3.2.4. Enrichment factors (EFs) and element fluxes in least abundant TE

We analyze here the biogeochemical behavior of the least abundant TE in the sinking particles, before, during, and after the dust event (Tables 3a-3d and Figures 2b-2e).

We have classified the minor TE according to their EF values: EF>1 (category a), approximately 1 (category b) and <1 (category c). However, to account for uncertainties due to local variability, we consider EF>1.5 and EF <0.7 to be more statistically robust but will discuss all the results.

a) Elements with EF values >1.0 in the trap particles collected during the dust intrusion.

The TE in this category are scavenged from the water column while the dust particles are sinking and include P, K, Mn, Ga, As, Br, Rb, Sr, I, Ba, La, Th and U. From this list only As, Br, Sr and I have EF values higher than 1.5 (Figure 2c), which illustrate the same behavior for P, Mn and Ba.

It is especially significant for Br and I (Figure 2d) to reach EF values of 20-40 during the dust event.

This finding is in agreement with the expected removal of I and Br from their dissolved phases within the upper layers of the water column (Steele & Thorpe, 2010). It is also worth noting that the removal of these elements from the water column is not directly related to the particle affinity/adsorption coefficient of all these elements. Consequently, Th, which is strongly particle reactive, is included in this category, however, Pb, also through very particle reactive has the opposite behavior. On the contrary, this category includes U, whose reactivity depends on its oxidation state, and Sr, which is conservative in seawater.

Contrasting with the major TE from the previous section, not all the elements change their EF before and during the dust event, and it is impossible to detect the changes attributed to the different origins of the particles (biological vs lithogenic). The EFs of Mn, As, Sr, Br and I (and to a lesser extent P, Rb and Ba) decrease during the dust event. Those of Ga and U do not show statistically significant changes from the pre-event to the dust event.

This distribution of EF is consistent at 200 m and 1000 m for all the elements. The only elements not showing consistent behaviors at both depths are K and Th. For potassium the EFs seems to increase at 200 m-depth once the dust intrusion is detected; no differences were found at 1000 m-depth. In the case of Th, no relevant differences were found at 200 m-depth, but they seem to slightly decrease at 1000 m-depth.

Within category a, the integrated vertical fluxes during the dust event of many of the elements (K, Mn, Ga, As, Br, Rb, Sr, Ba and Th) were observed as being higher at 1000 m-depth than at 200 m-depth (Table 4a, 4b). However, the elements As, Ba and Th reflect relevant differences higher than 20% and could account for local variabilities. The mentioned elements have very different biogeochemical behaviors such as micronutrients-like elements (Mn, Ga, Ba, La), particle reactive elements (Th), and conservative elements (K and U).

The combination of EF>1 and increased vertical flux from 200 m to 1000 m during the dust event indicates that when the dust particles sank, they likely removed the above-mentioned elements from the water column. If the sinking dust particles were remineralized in the mesopelagic zone, these elements were associated to the refractory phase of the dust particles and were therefore not released back to the water column, resulting in a net increase of these specific element fluxes from 200 m to 1000 m. However, it is important to remember that this net removal during the dust event is only statistically robust for As, Ba and Th. Iodine is an exception; the element fluxes integrated for the dust period decreased from 200 m to 1000 m, but its EF at 200 m was less than 1. This suggests that dust particles can remove a certain amount of I from the water column within the euphotic layer, but

401 then, during remineralization of the sinking dust particles from 200 m to 1000 m, a certain fraction of
402 this I is released back to the water column. This may be explained if I is associated with the most
403 labile form of the sinking particles, possibly the biogenic phase. Previous work has suggested that
404 less than 3% of the particulate iodine present in the upper layer of the North Atlantic Ocean reaches
405 the sediment (Wong et al., 1976). Indeed, the vertical fluxes reported by Wong et al. (1976) as
406 suspended particles were in the range of 0.4 mg m^{-2} d^{-1}, almost two orders of magnitude below the
407 fluxes shown in this work.
408
409 When element fluxes are integrated for the whole sampling season, some elements (Mn also Br, Ba,
410 La) present an increasing flux from 200 m to 1000 m. This implies that Mn, Br, Ba and La are
411 associated with a more refractory phase. Most other element fluxes (P, K, Ga, As, Rb, Sr, I, Th and
412 U) decrease from 200 m to 1000 m. This suggests they are associated with a labile phase and
413 released to the water column during remineralization.
414
415 The observed TE fluxes suggest that the compositions of sinking particles are, as expected, different
416 during a season than during the dust event. Biogenic, particles that sink during the season, outside of
417 the dust event, are labile and more easily remineralized. Element flux from 200 m to 1000 m
418 decreases during the season because the elements associated to this labile phase are remineralized
419 back to the water column.
420
421 b) Elements having EF values ≈ 1.0 in the trap particles collected during the dust intrusion.
422 This category corresponds to TE that are not being removed from the water column by the dust
423 particles when they sink. This attribute was observed in the elements V, Y, Zr, Nb, Ce, and Y.
424 (Figure 2d). Note that Y's particle reactivity.
425
426 There is a clear change in the EF before and during the dust event for Y and Zr, as their EFs
427 increases at both sampling depths. The values for V remain constant (inside the uncertainty intervals)
428 at both depths. The EFs of Nb (and Ce) show different temporal trends at different depths; the values
429 increase for Nb (decrease for Ce) at 200 m-depth with the arrival of the dust event but remain
430 constant at the 1000 m-depth level.
431
432 During SD-1, all (category b) TE integrated fluxes increased with depth. Based on the EF values and
433 these increasing fluxes, we conclude that all elements (V, Y, Zr, Nb and Ce) passed through the

mesopelagic, without any remarkable interaction with the water column since EF ≅ 1. Additionally, we were able to confirm the refractory nature of the dust sinking particles for this (category b).

In (category b), when the vertical fluxes were integrated for the complete data series including SD-1, the integrated flux decreased from 200 m to 1000 m for V by ~10%. There are no differences within the uncertainty intervals for Nb and Ce. There is only slight reduction found for Y (2%) and Zr (4%), therefore for this reason results are not conclusive for these two elements. We conclude that Nb and Ce are associated to the most refractory phase of the sinking particles, while V, Y and Zr are more labile for the organic sinking particles.

c) Elements having values < 1.0 in the trap particles collected during the dust intrusion.

This category includes the elements Cr, Ni, Cu, Zn, Sn, and Pb, all of which, excluding Ni and Pb, have EF values below 0.7 (Figure 2e). This indicates that, when sinking, the particles are sources of these elements, and therefore increase their abundance in the dissolved phase. All these elements decrease their EF values before and during the dust event. Furthermore, the EF values for these elements have the same behavior at 200 m and 1000 m.

Finally, the (category c) corresponds to elements that were released from the sinking particles to the water column in the first 200 m based on EF<1. However, the vertical fluxes increase significantly from 200 m to 1000 m-depth for all the TE except for Cr. For (category c), when vertical fluxes were integrated for the complete data series, the Cu and Sn integrated fluxes increased from 200 m to 1000 m by ~22 and 15%, respectively.

During the dust event, there was a remarkable asymmetry for the elements of (category c) with EF < 1 at 200 m and increasing fluxes from 200 m to 1000 m. Iodine was only exception with EF>1 decreased flux from 200 m to 1000 m. These asymmetries indicate that more complex mechanisms that should be further analyzed, e.g. remineralization and differences in particulate properties at 200 m and at 1000 m, phytoplankton and zooplankton abundance, stratification. Furthermore, future investigations should consider the mentioned different sources of uncertainty in order to improve the accuracy of these conclusions.

3.3. Comparisons with previous studies

Heimbürger et al. (2013) provided average daily fluxes for Cr, Cu, Ni, Zn and Pb using sediment traps deployed at the DYFAMED site, at 2380 m-depth, for nearly one year. The values from Heimbürger et al. (2013) are of the same order of magnitude as those measured in this work (Supplementary Material). Heimbürger et al. (2012) also provided an estimation of daily fluxes using data from the upper layer of sediment cores collected at the same site. Those fluxes are approximately 3-4 times lower than maximum values measured in our sediment traps at 1000 m-depth during the dust intrusion event. Heimbürger et al., (2014) compiled yearly vertical flux averages for the period 2004-2007. We compared our data from the February 2004 dust event with these yearly vertical fluxes and confirm that a single large dust event, such as the one analyzed in this work, produces a significant proportion of the total average annual flux: 45 % (Cu), 60-70% (Al, Ni, Zn, Cr), 80-85% (Mn and Pb), or 115% (Fe). These calculations agree with the data provided by Pham et al. (2017) for artificial radionuclides (^{137}Cs and $^{239/240}$Pu) in the same sample set.

In the case of the element La, vertical daily fluxes during the February 2004 dust event are between one and two orders of magnitude higher than those registered at the Gulf of Lions by Fowler et al. (1992).

4. Summary and conclusions

A major Saharan dust deposition event was detected at Monaco in 20th February 2004, and, in a few days , the sinking particle flux at 200 m depth increased by more than one order of magnitude, (1200 mg m^{-2} d^{-1} the highest flux measured to date at the DYFAMED sediment traps). At 1000 m depth, the dust event was detected from February to mid April 2004.

We estimated the sinking velocity of dust particles at the DYFAMED site to be > 20 m d^{-1} for the slow particles and < 250 m d^{-1} for the fastest dust particles, based on the particle mass flux and travelling time of sinking particles during 3 weeks at 200 m and 4 weeks at 1000 m depth.

For the 30 elements analyzed, except for I, the dust event did not enhance dissolved inventories in the water column, since the sinking dust particles scavenged the elements from the water column as they sank. The results suggest that remineralization of the sinking dust particles did not occur between 200 m and 1000 m-water depth, and that sinking dust particles scavenged dissolved TE

from the water column.

We also integrated element fluxes for the complete sampling season prior, during, and after SD-1 event. For many of the analyzed elements, the fluxes decreased from 200 m to 1000 m, which contrasts strongly with the increased fluxes detected during the dust event. This implies that the composition of the sinking particles is different during the period of dust event. Dust particles are refractory and for this reason, the remineralization of the sinking dust particles was likely weak and slow. Biogenic, particles that sink during this period, are labile and more easily remineralized. Element flux from 200 m to 1000 m decreases during the season because the elements associated to this labile phase are remineralized and recycled back to the water column.

Acknowledgments:

The IAEA is grateful for the support provided to its Environment Laboratories by the Government of the Principality of Monaco. The authors are acknowledged to the editorial team of Marine Chemistry for their support and flexibility. Special acknowledgement must be expressed to the reviewers of the manuscript. Their questions and suggestions, and their open attitude, dedication and scientific rigor helped us to qualitatively improve this manuscript. The authors are grateful to the S. Morris and M. Lebrec for the final English revision.

References

Baskaran, M., 2011. Handbook of Environmental Isotope Geochemistry, Media.

Béthoux, J.P., Morin, P., Ruiz-Pino, D.P., 2002. Temporal trends in nutrient ratios: chemical evidence of Mediterranean ecosystem changes driven by human activity. Deep Sea Res. Part II Top. Stud. Oceanogr. 49, 2007–2016. doi:10.1016/S0967-0645(02)00024-3

Buat-Menard, P., Lambert, C.E., 1993. Overview of the DYFAMED program. Ann. - Inst. Oceanogr. Paris 69.

Coppola, L., Diamond Riquier, E., Carval, T. (2019). Dyfamed observatory data. SEANOE. http://doi.org/10.17882/43749

533 Fowler, S. W., Hamilton, T. F., Peinert, Rolf, La Rosa, J. and Teyssie, J.-L. (1992) The vertical
534 flux of rare earth elements in the northwestern Mediterranean. Open Access In: EROS 2000
535 (European river ocean system) third workshop of the north-west Mediterranean Sea., ed. by
536 Martin, J. M. and Barth, H.. Water Pollution Research Reports, 28. Commission of the European
537 Communities, Brussels, Belgium, pp. 401-412. ISBN 2872630791
538
539 Gross, A., Palchan, D., Krom, M.D., Angert, A., 2016. Elemental and isotopic composition of
540 surface soils from key Saharan dust sources. Chem. Geol. 442, 54–61.
541 doi:10.1016/j.chemgeo.2016.09.001
542
543 Guerzoni, S., Chester, R., Dulac, F., Herut, B., Loÿe-Pilot, M.-D., Measures, C., Migon, C.,
544 Molinaroli, E., Moulin, C., Rossini, P., Saydam, C., Soudine, A., Ziveri, P., 1999. The role of
545 atmospheric deposition in the biogeochemistry of the Mediterranean Sea. Prog. Oceanogr. 44,
546 147–
547 190. doi:10.1016/S0079-6611(99)00024-5.
548
549 Heimbürger, L., Cossa, D., Thibodeau, B., 2012. Natural and anthropogenic trace metals in
550 sediments of the Ligurian Sea (Northwestern Mediterranean). Chem. Geol. 291, 141–151.
551 doi:10.1016/j.chemgeo.2011.10.011
552
553 Heimbürger, L.E., Lavigne, H., Migon, C., D'Ortenzio, F., Estournel, C., Coppola, L., Miquel,
554 J.C., 2013. Temporal variability of vertical export flux at the DYFAMED time-series station
555 (Northwestern Mediterranean Sea). Prog. Oceanogr. 119, 59–67.
556 doi:10.1016/j.pocean.2013.08.005
557
558 Heimbürger, L.E., Migon, C., Losno, R., Miquel, J.C., Thibodeau, B., Stabholz, M., Dufour, A.,
559 Leblond, N., 2014. Vertical export flux of metals in the Mediterranean Sea. Deep. Res. Part I
560 Oceanogr. Res. Pap. 87, 14–23. doi:10.1016/j.dsr.2014.02.001
561
562 Heussner, S., Ratti, C., Carbonne, J., 1990. The PPS 3 time-series sediment trap and the trap
563 sample processing techniques used during the ECOMARGE experiment. Continental Shelf
564 Research, 10 (9-11), 943-958.
565
566 Jones, V., Meador, T.B., Gogou, A., Migon, C., Penkman, K.E.H., Collins, M.J., Repeta, D.J.,

2013. Characterisation and dynamics of dissolved organic matter in the Northwestern Mediterranean Sea. Prog. Oceanogr. 119, 78–89. doi:10.1016/j.pocean.2013.06.007

Karl, D.M., Lukas, R., 1996. The Hawaii Ocean Time-series (HOT) program: Background, rationale and field implementation. Deep-Sea Research II 43, 129-156.

Le Moigne, F.A.C., Villa-Alfageme, M., Sanders, R.J., Marsay, C., Henson, S., García-Tenorio, R., 2013. Export of organic carbon and biominerals derived from 234Th and 210Po at the Porcupine Abyssal Plain. Deep Sea Res. I 72, 88-101.

Marconi, M., Sferlazzo, D.M., Becagli, S., Bommarito, C., Calzolai, G., Chiari, M., Di Sarra, A., Ghedini, C., Gómez-Amo, J.L., Lucarelli, F., Meloni, D., Monteleone, F., Nava, S., Pace, G., Piacentino, S., Rugi, F., Severi, M., Traversi, R., Udisti, R., 2014. Saharan dust aerosol over the central Mediterranean Sea: PM10 chemical composition and concentration versus optical columnar measurements. Atmos. Chem. Phys. 14, 2039–2054. doi:10.5194/acp-14-2039-2014

Martín, J., Sanchez-Cabeza, J.A., Eriksson, M., Levy, I., Miquel, J.C., 2009. Recent accumulation of trace metals in sediments at the DYFAMED site (Northwestern Mediterranean Sea). Mar. Pollut. Bull. 59, 146–153. doi:10.1016/j.marpolbul.2009.03.013

Martín, J., Miquel, J.C., Khripounoff, A., 2010. Impact of open sea deep convection on sediment remobilization in the western Mediterranean. Geophys. Res. Lett. 37, 1–6. doi:10.1029/2010GL043704

Migeon, S., Mulder, T., Savoye, B., Sage, F., 2006. The Var turbidite system (Ligurian sea, northwestern Mediterranean) - Morphology, sediment supply, construction of turbidite levee and sediment waves: Implications for hydrocarbon reservoirs. Geo-Marine Lett. 26, 361–371. doi:10.1007/s00367-006-0047-x

Migon, C., Journel, B., Nicolas, E., 1997. Measurement of trace metal wet, dry and total atmospheric fluxes over the Ligurian Sea. Atmos. Environ. 31, 889–896. doi:10.1016/S1352-2310(96)00242-7

Migon, C., Sandroni, V., Marty, J.-C., Gasser, B., Miquel, J.-C., 2002. Transfer of atmospheric

601 matter through the euphotic layer in the northwestern Mediterranean: seasonal pattern and driving
602 forces. Deep Sea Res. Part II Top. Stud. Oceanogr. 49, 2125–2141. doi:10.1016/S0967-
603 0645(02)00031-0
604
605 Miquel, J.C., Martín, J., Gasser, B., Rodriguez-y-Baena, A., Toubal, T., Fowler, S.W., 2011.
606 Dynamics of particle flux and carbon export in the northwestern Mediterranean Sea: A two
607 decade time-series study at the DYFAMED site. Prog. Oceanogr. 91, 461–481.
608 doi:10.1016/j.pocean.2011.07.018
609
610 Moreno, A., Cacho, I., Canals, M., Grimalt, J.O., Sánchez-Goñi, M.F., Shackleton, N., Sierro,
611 F.J., 2005. Links between marine and atmospheric processes oscillating on a millennial time-
612 scale. A multi-proxy study of the last 50,000yr from the Alboran Sea (Western Mediterranean
613 Sea). Quat. Sci. Rev. 24, 1623–1636. doi:10.1016/j.quascirev.2004.06.018
614
615 Pasqueron de Fommervault, O., Migon, C., D'Ortenzio, F., Ribera d'Alcalá, M., Coppola, L.,
616 2015. Temporal variability of nutrient concentrations in the northwestern Mediterranean sea
617 (DYFAMED time-series station). Deep. Sea Res. Part I Oceanogr. Res. Pap. 100, 1–12.
618 doi:10.1016/j.dsr.2015.02.006
619 Pham, M.K., Povinec, P.P., Lee, S.H., Oregioni, B., 2003. Atmospheric transport of particles from
620 the North Africa to Monaco. Bull. du Bur. Natl. Metrol. 2003–2, 143–149.
621
622 Pham, M.K., Chamizo, E., Mas Balbuena, J.L., Miquel, J.-C., Martín, J., Osvath, I., Povinec, P.P.,
623 2017. Impact of Saharan dust events on radionuclide levels in Monaco air and in the water
624 column of the northwest Mediterranean Sea. J. Environ. Radioact. 166, 2–9.
625 doi:10.1016/j.jenvrad.2016.04.014
626
627 Scheuvens, D., Schültz, L., Kandler, K., Ebert, M., Weinbruch, S., 2013. Bulk composition of
628 northern African dust and its source sediments - A compilation. Earth-Science Rev. 116, 170–
629 194. doi:10.1016/j.earscirev.2012.08.005
630
631 Schlitzer, R. et al., 2018. The GEOTRACES Intermediate Data Product 2017. Chem. Geol. 493,
632 210-223.
633
634 Steele, J.H., Thorpe, S.A., 2010. Marine Chemistry & Geochemistry, 2nd ed. Elsevier Ltd,

635 London.
636
637 Steinberg, D.K., Carlson, C.A., Bates, N.R., Johnson, R.J., Michaels, A.F., Knap, A.H., 2001.
638 Overview of the US JGOFS Bermuda Atlantic Time-series Study (BATS): a decade-scale look at
639 ocean biology and biogeochemistry. Deep-Sea Research II, 48, 1405–1447.
640
641 Ternon, E., Guieu, C., Loÿe-Pilot, M.-D., Leblond, N., Bosc, E., Gasser, B., Miquel, J.-C., Martín,
642 J. 2010. The impact of Saharan dust on the particulate export in the water column of the
643 NorthWestern Mediterranean Sea. Biogeosciences, 7, 809–826. doi: 10.5194/bg-7-809-2010.
644
645 Villa-Alfageme, M., De Soto, F., Le Moigne, F.A.C., Giering, S.L.C., Sanders, R., García-
646 Tenorio, R. (2014). Observations and modeling of slow-sinking particles in the twilight zone.
647 Global Biogeochemical Cycles, 28 (11), 1327-1342. DOI: 10.1002/2014GB004981
648
649 Villa-Alfageme, M., de Soto, F.C., Ceballos, E., Giering, S.L.C., LeMoigne, F.A.C., Henson, S.,
650 Mas, J.L., Sanders, R.J., 2016. Geographical, seasonal, and depth variation in sinking particle
651 speeds in the North Atlantic. Geophysical Research Letters, 43, 8609-8616. doi:
652 10.1002/2016GL069233
653
654 Wong, G.T.F., Brewer, P.G., Spencer, D.W., 1976. The distribution of particulate iodine in the
655 Atlantic Ocean. Earth Planet Sci. Let. 32, 441-450. doi:10.1016/j.marchem.2007.03.003
656
657 Wedepohl, K. H., 1995. The composition of the continental crust. Geochim. et Cosmochim. Acta 59,
658 1217-1232.
659

Figure 1: Location of the DYFAMED and IAEA-EL sampling sites.

Figure 2.a: Particle flux during the sampling campaign at 200 m and 1000 m-depth at DYFAMED station. Red line indicates the detection of the dust event at IAEA-EL. Note that the particle flux represents the collection of 15 days. Thus, the dust event starts on the 20th February, but the associated particle flux is displayed from 15th to 29th February.

Figure 2.b: Enrichment Factors found in sediment trap samples at 200 m and 1000 m-depth for Si, Ca, Ti and Fe. Red line indicates the detection of the dust event at IAEA-EL. The elements are not shown in order of increasing atomic number, but keeping the order of the discussion in the text. Each point corresponds to the average of two weeks sampling interval and are the data points are displayed on the mid-day of the two weeks.

Figure 2.c: Enrichment Factors found in sediment trap samples at 200 m and 1000 m-depth for P, Mn, Sr and Ba. Red line indicates the detection of the dust event at IAEA-EL. The elements are not shown in order of increasing atomic number, but keeping the order of the discussion in the text. Each point corresponds to the average of two weeks sampling interval and are the data points are displayed on the mid-day of the two weeks.

Figure 2.d: Enrichment Factors found in sediment trap samples at 200 m and 1000 m-depth for V, Br, Zr and I. Red line indicates the detection of the dust event at IAEA-EL. The elements are not shown in order of increasing atomic number, but keeping the order of the discussion in the text. Each point corresponds to the average of two weeks sampling interval and are the data points are displayed on the mid-day of the two weeks.

Figure 2.e: Enrichment Factors found in sediment trap samples at 200 m and 1000 m-depth for Cu, Zn, Sn and Pb. Red line indicates the detection of the dust event at IAEA-EL. The elements are not shown in order of increasing atomic number, but keeping the order of the discussion in the text. Each point corresponds to the average of two weeks sampling interval and are the data points are displayed on the mid-day of the two weeks.

Figure 3: Zr/Al mass ratios found in sediment trap samples collected at 200m and 1000m-depth.

Figure 4.a: Mass flux and element vertical fluxes of Si, Ca, Ti and Fe observed at the DYFAMED site (200 m-depth). Note the different scales and different units. Ca and Fe fluxes have been divided by 10, and S by 100, in order to keep the same numeric scale. Each point corresponds to the average of two weeks sampling interval and are the data points are displayed on the mid-day of the two weeks.

Figure 4.b: Mass flux and element vertical fluxes of Si, Ca, Ti and Fe observed at the DYFAMED site (1000 m-depth). Note the different scales and different units. Ca and Fe fluxes have been divided by 10, and S by 100, in order to keep the same numeric scale. Each point corresponds to the average of two weeks sampling interval and are the data points are displayed on the mid-day of the two weeks.

Figure-1

Click here to access/download;Figure;Figure 1_situation map.jpg

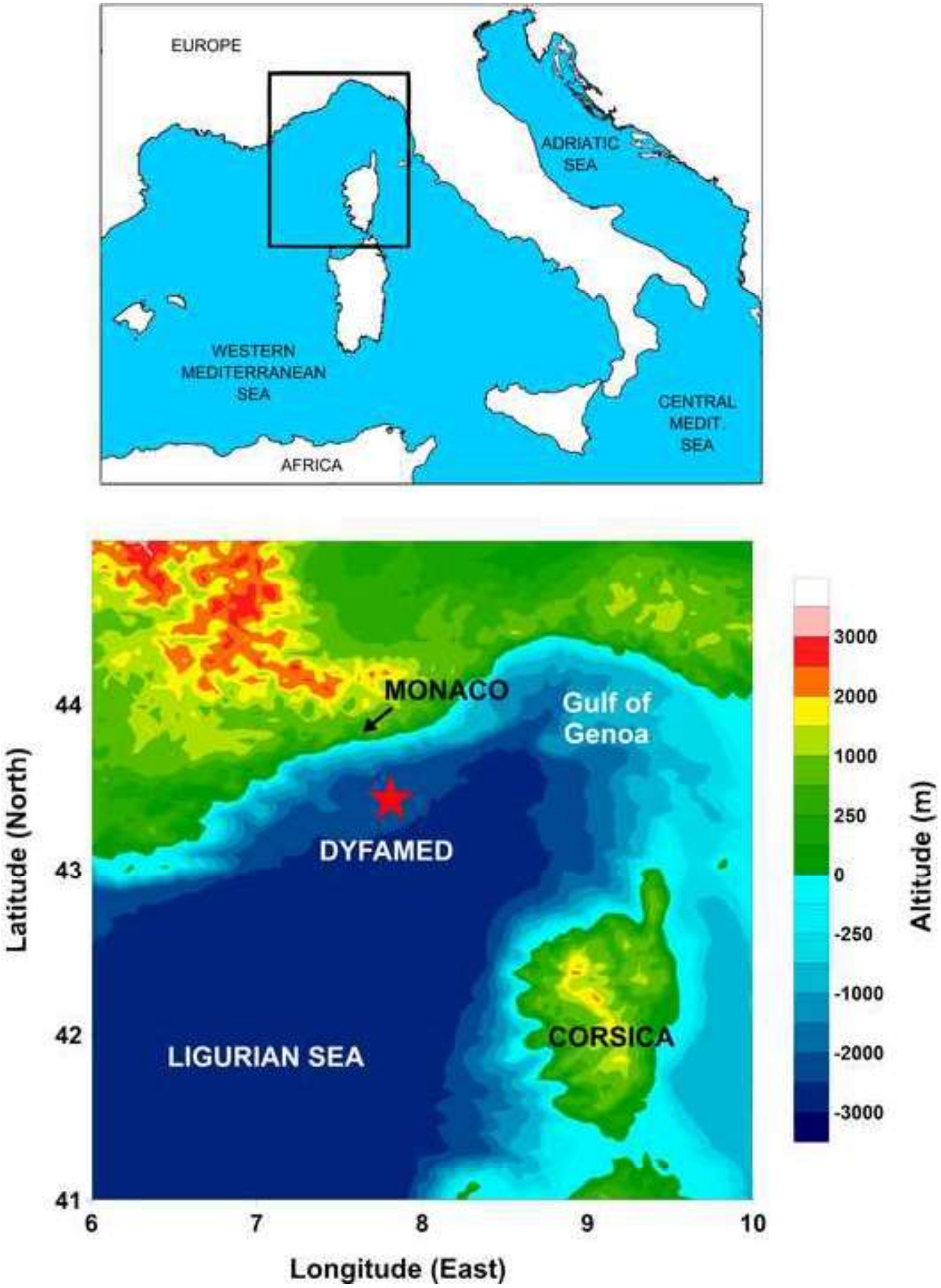

Figure-2a

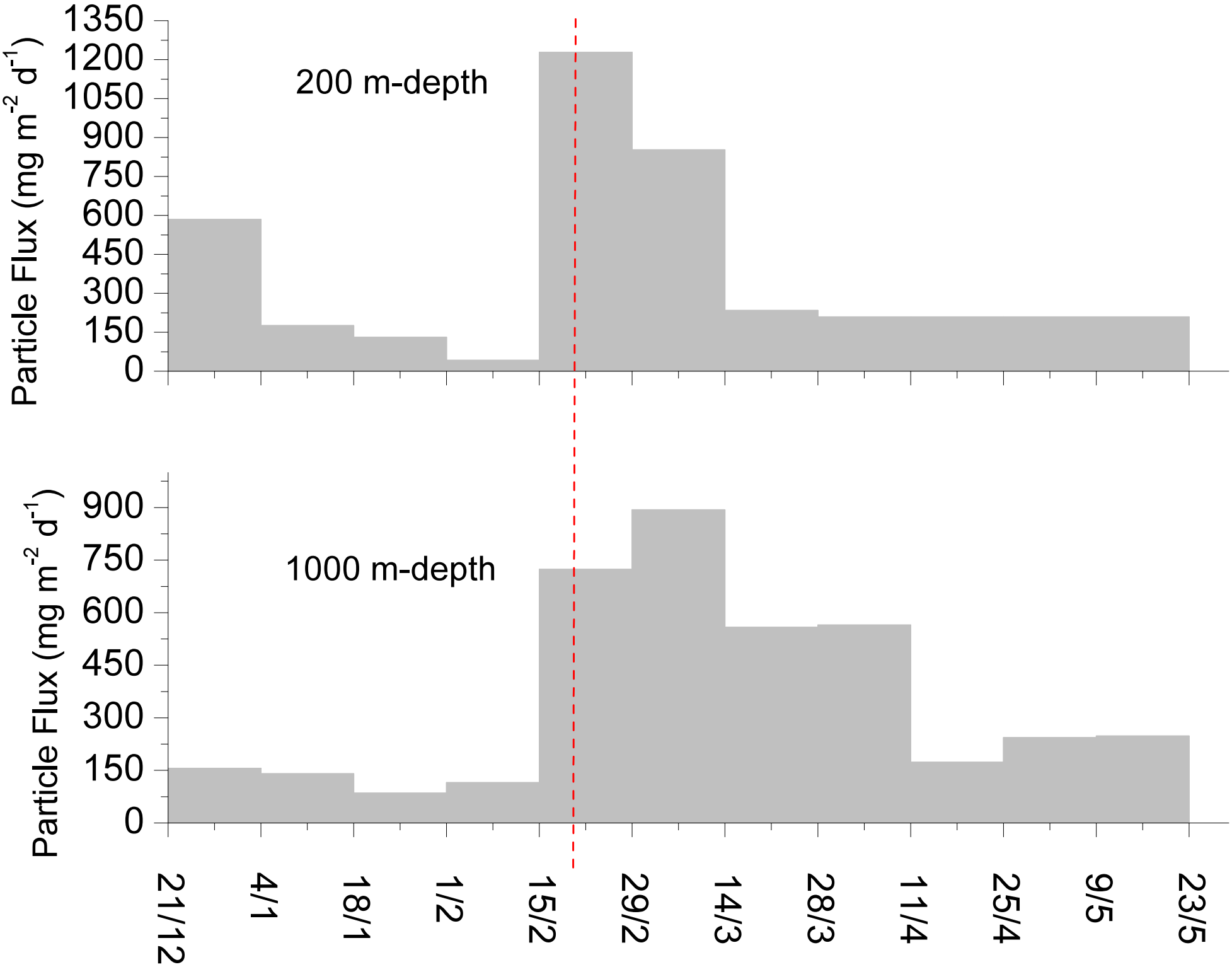
200 m-depth
Particle Flux (mg m-2 d-1)
1350
1200
1050
900
750
600
450
300
150
0
1000 m-depth
Particle Flux (mg m-2 d-1)
900
750
600
450
300
150
0
21/12
4/1
18/1
1/2
15/2
29/2
14/3
28/3
11/4
25/4
9/5
23/5

Figure-2b

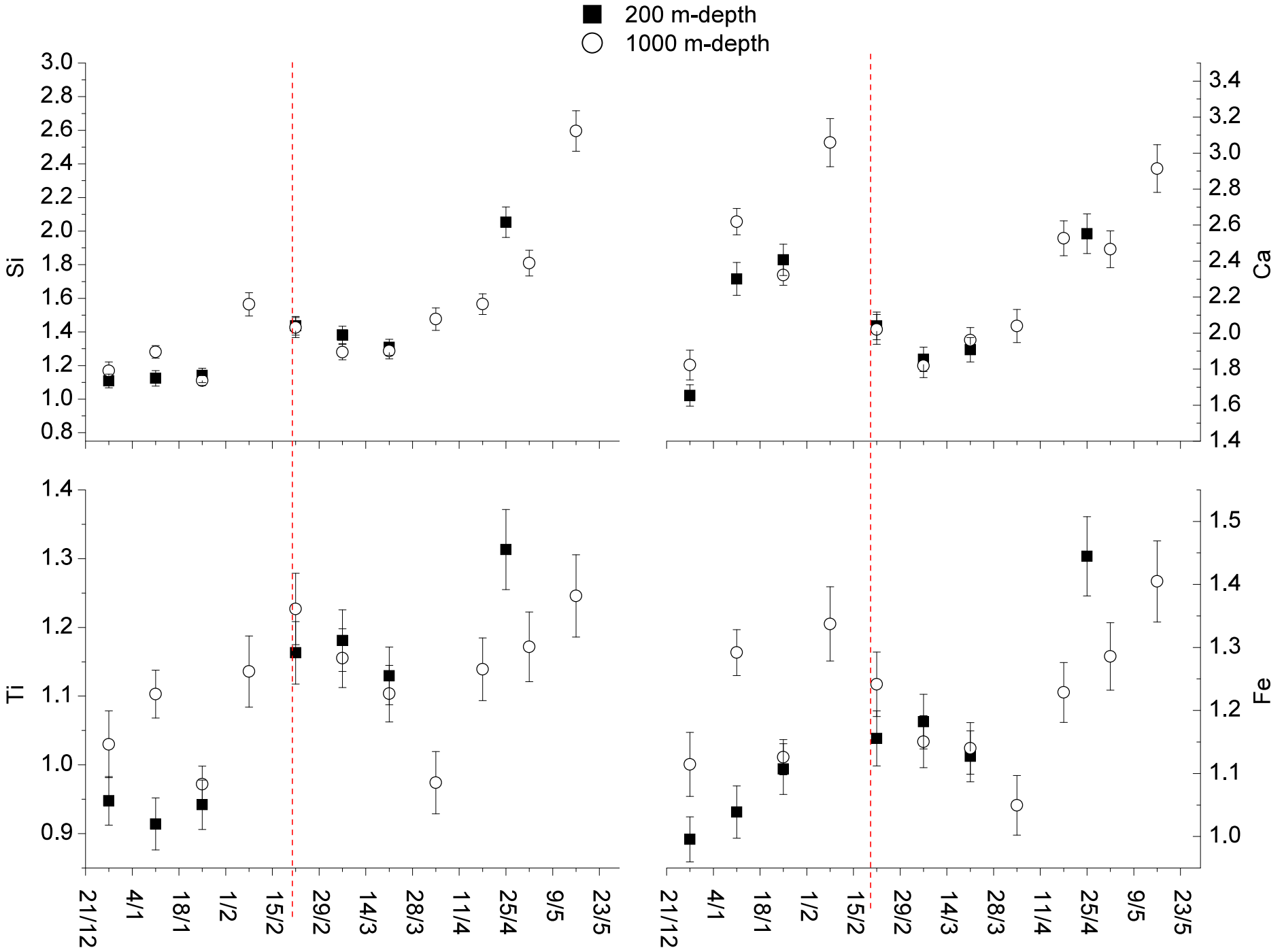
200 m-depth
1000 m-depth
Si
Ca
Ti
Fe
21/12
4/1
18/1
1/2
15/2
29/2
14/3
28/3
11/4
25/4
9/5
23/5

Figure-2c

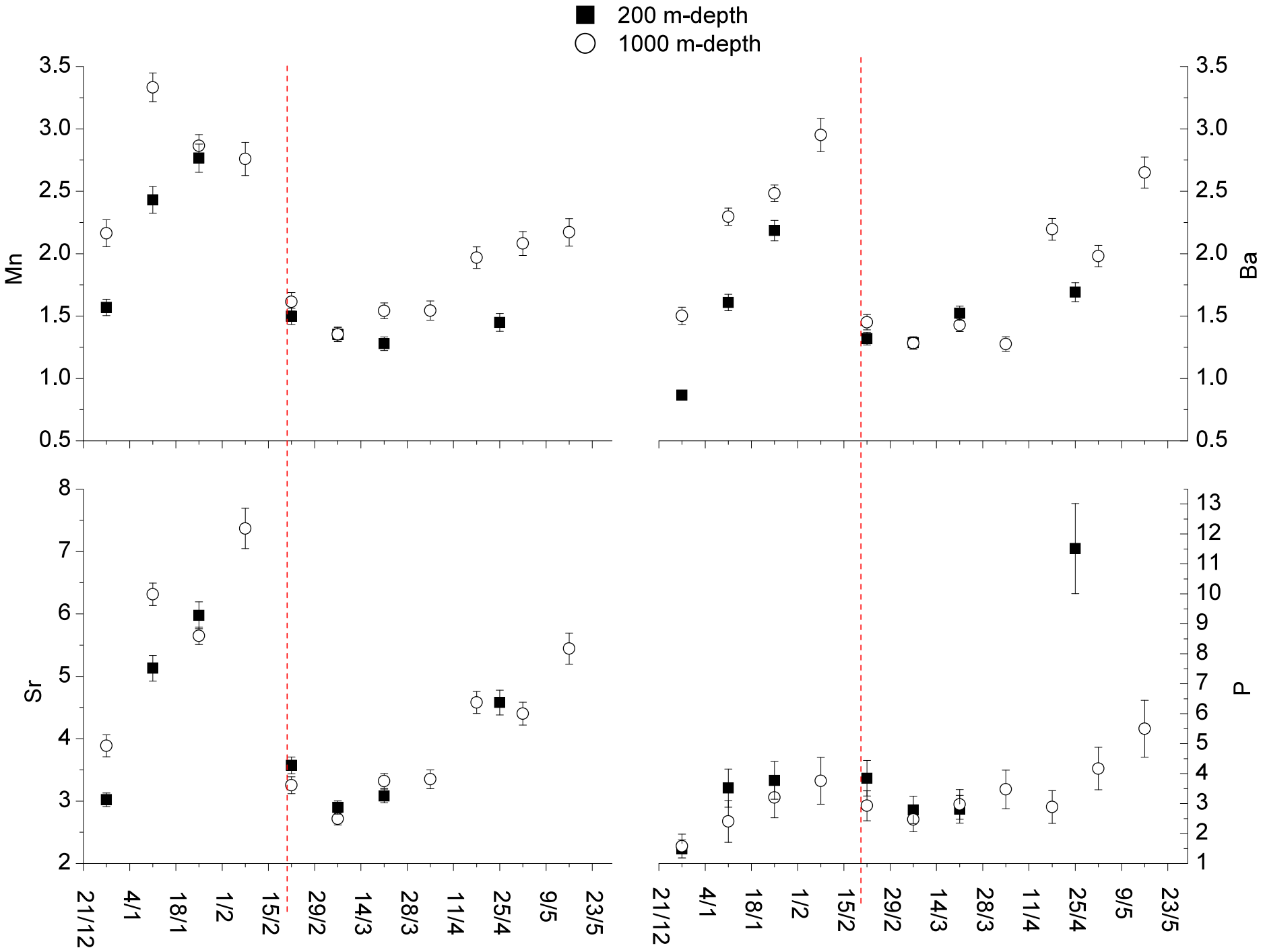
200 m-depth
1000 m-depth
Mn
Ba
Sr
P
21/12
4/1
18/1
1/2
15/2
29/2
14/3
28/3
11/4
25/4
9/5
23/5

Figure-2d

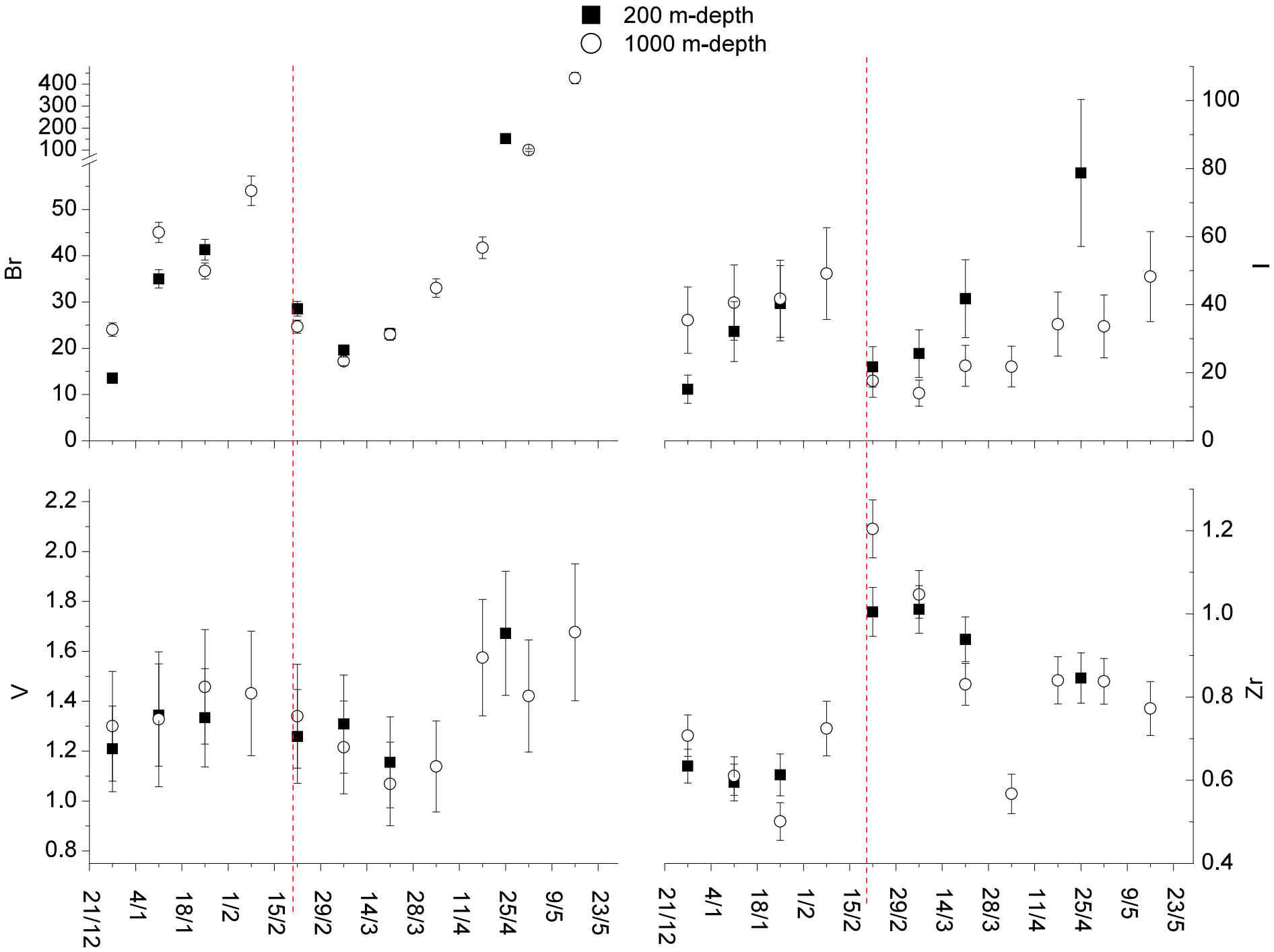
200 m-depth
1000 m-depth
BR
I
V
Zr
400
300
200
100
50
40
30
20
10
0
100
80
60
40
20
0
2.2
2.0
1.8
1.6
1.4
1.2
1.0
0.8
1.2
1.0
0.8
0.6
0.4
21/12
4/1
18/1
1/2
15/2
29/2
14/3
28/3
11/4
25/4
9/5
23/5

Figure-2e

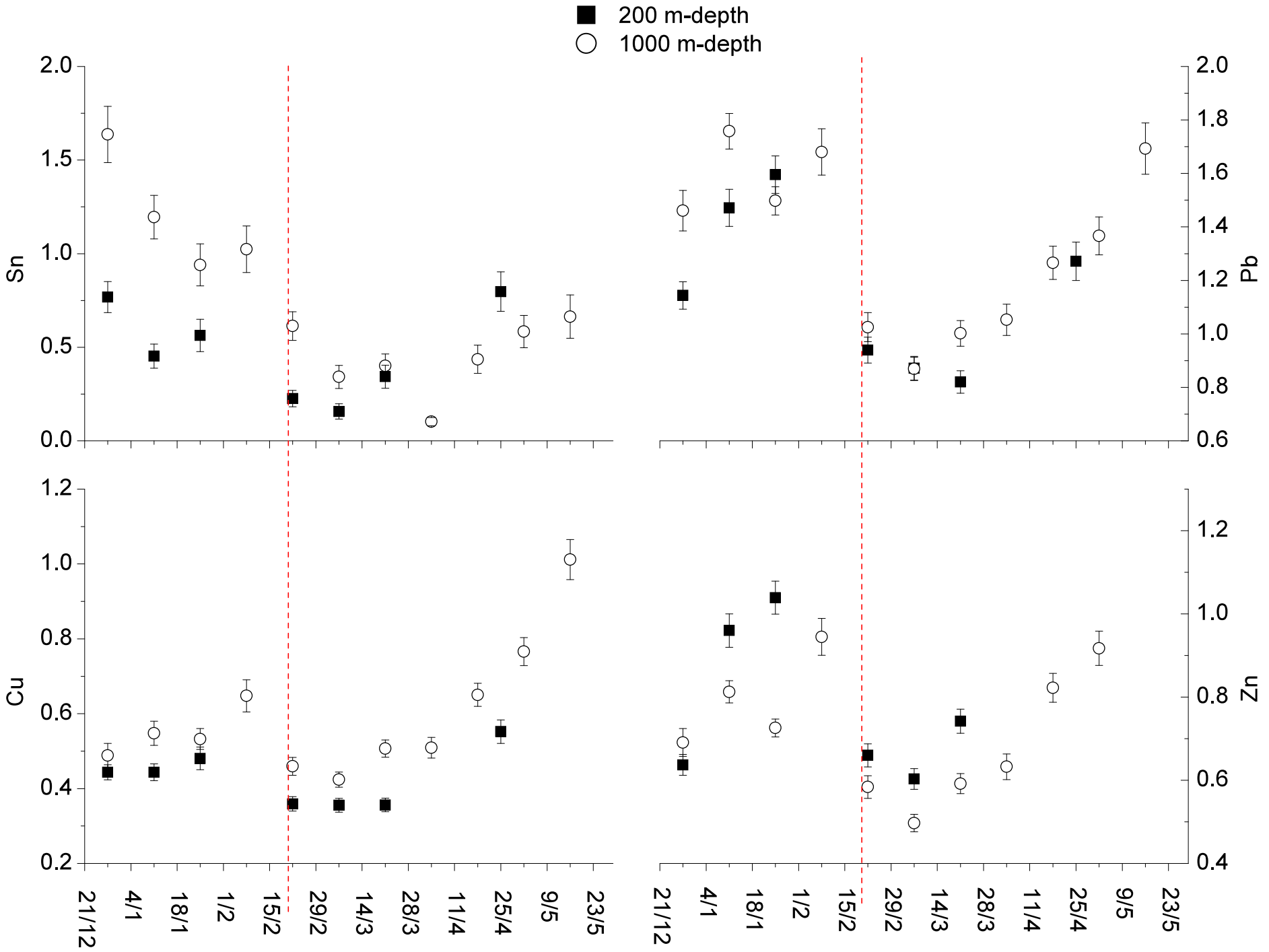
200 m-depth
1000 m-depth
Sn
Pb
Cu
Zn
2.0
1.5
1.0
0.5
0.0
1.8
1.6
1.4
1.2
0.8
0.6
0.4
0.2
21/12
4/1
18/1
1/2
15/2
29/2
14/3
28/3
11/4
25/4
9/5
23/5

Figure-3

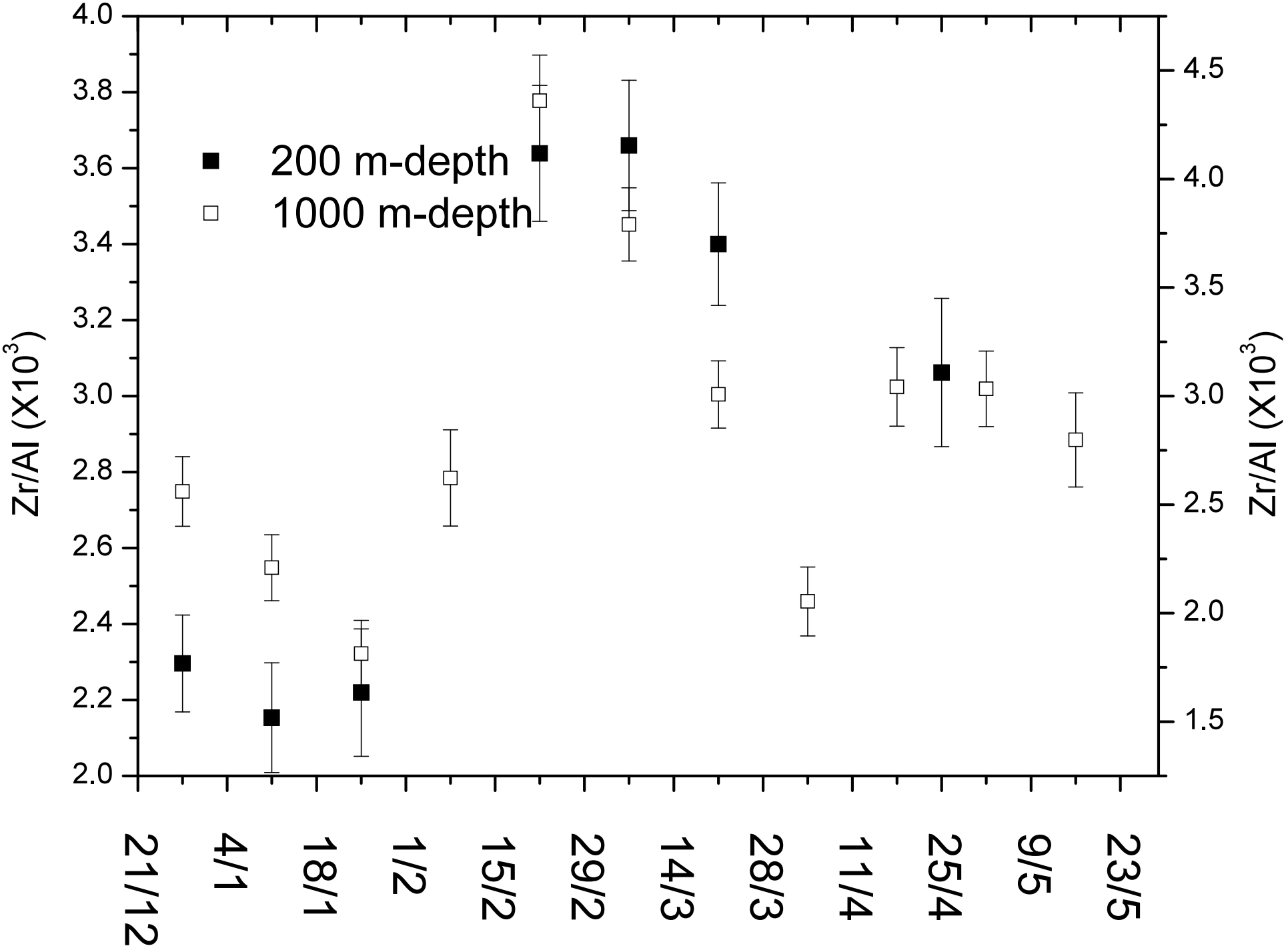
200 m-depth
1000 m-depth
Zr/Al (X10^3)
Zr/Al (X10^3)
4.0
3.8
3.6
3.4
3.2
3.0
2.8
2.6
2.4
2.2
2.0
4.5
4.0
3.5
3.0
2.5
2.0
1.5
21/12
4/1
18/1
1/2
15/2
29/2
14/3
28/3
11/4
25/4
9/5
23/5

Figure-4a

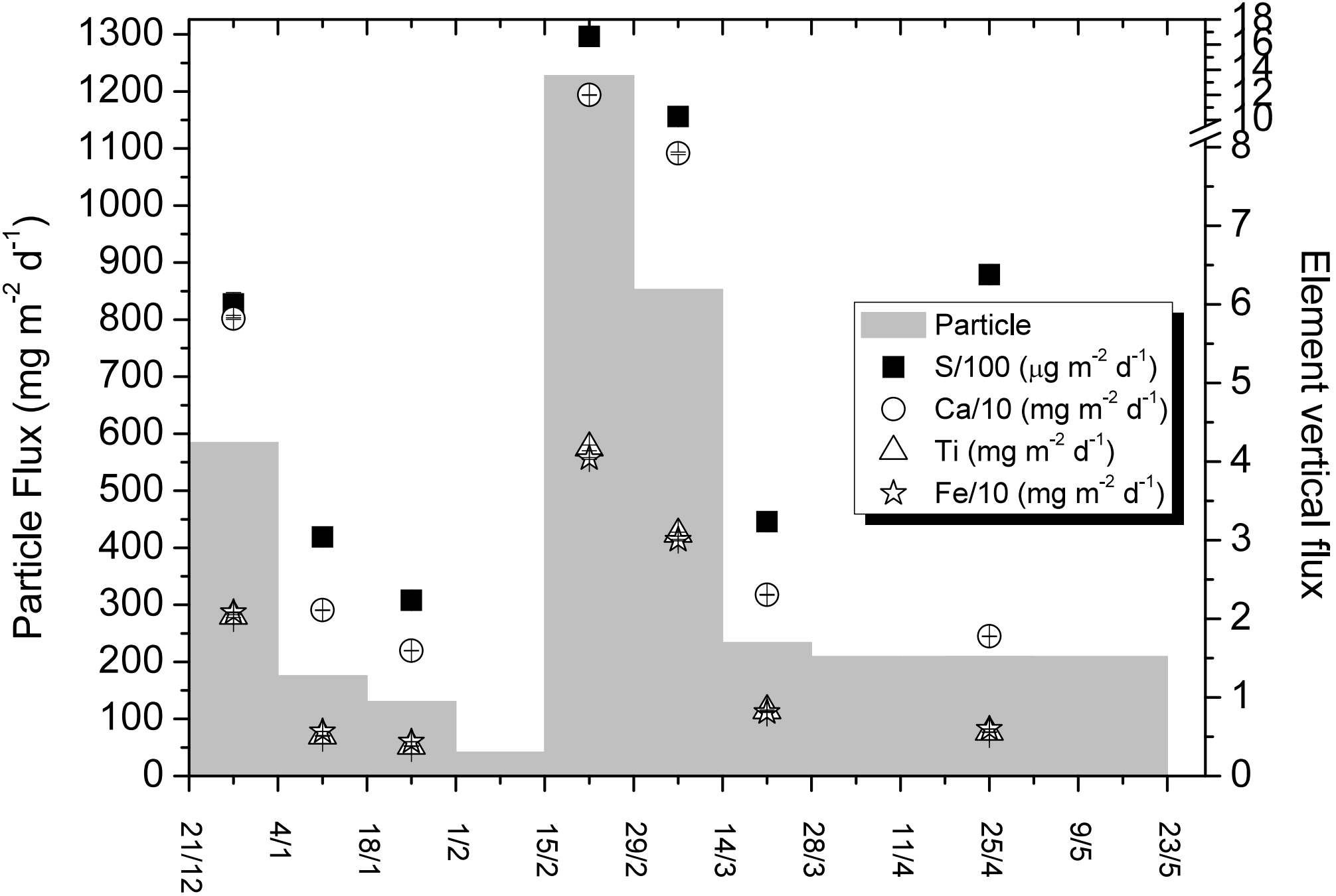
Particle Flux (mg m-2 d-1)
Element vertical flux
Particle
S/100 (μg m-2 d-1)
Ca/10 (mg m-2 d-1)
Ti (mg m-2 d-1)
Fe/10 (mg m-2 d-1)
0
100
200
300
400
500
600
700
800
900
1000
1100
1200
1300
0
1
2
3
4
5
6
7
8
21/12
4/1
18/1
1/2
15/2
29/2
14/3
28/3
11/4
25/4
9/5
23/5

Figure-4b

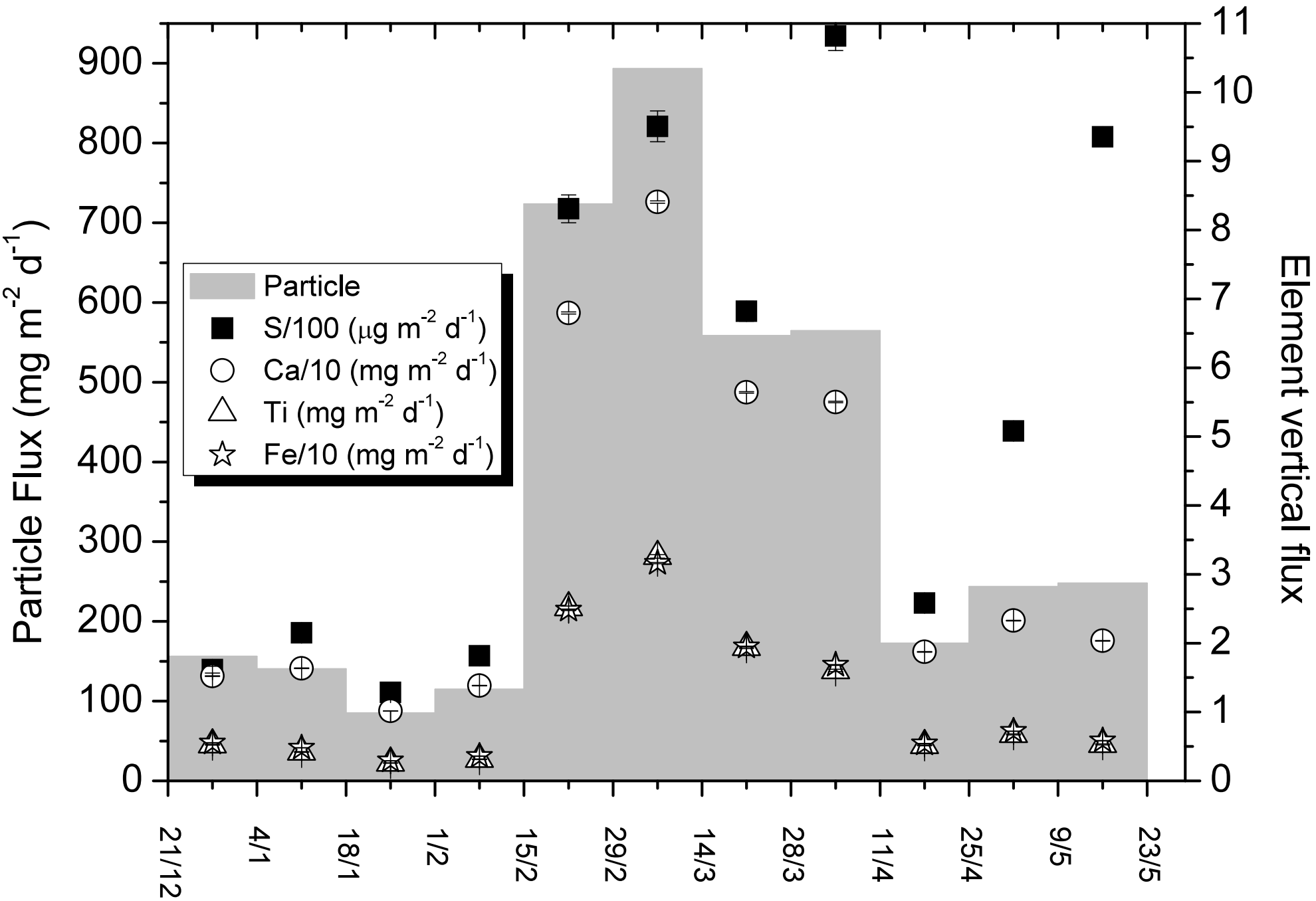
Particle Flux (mg m-2 d-1)
Element vertical flux
Particle
S/100 (μg m-2 d-1)
Ca/10 (mg m-2 d-1)
Ti (mg m-2 d-1)
Fe/10 (mg m-2 d-1)
0
100
200
300
400
500
600
700
800
900
0
1
2
3
4
5
6
7
8
9
10
11
21/12
4/1
18/1
1/2
15/2
29/2
14/3
28/3
11/4
25/4
9/5
23/5

Tables

Supplementary Material

Click here to access/download

Table

Supplementary material.docx

Supplementary material

Table i.a. Trace element composition of samples determined by X-ray Fluorescence (XRF; n= 1). Uncertainties provided for k = 1 (65.3% confidence interval).

Element	**Al**	**Si**	**S**	**P**	**K**	**Ca**	**Ti**	**V**
Sample	mg/g	mg/g	µg/g	µg/g	µg/g	mg/g	mg/g	µg/g
Atmospheric dust.								
SD1	53.3±1.0	162±1	919±20	173±18	19.6±0.1	68.8±0.2	4.20±0.03	105±10
SD2	46.8±1.1	152±1	1018±19	334±24	18.1±0.1	46.4±0.1	4.27±0.03	100±10
Sediment traps, 200 m-depth.								
ST2	46.6±1.4	157±1	1027±25	225±38	21.6±0.1	99.5±0.2	3.48±0.03	111±11
ST3	40.4±1.4	138±1	1730±34	461±66	17.9±0.1	120.0±0.2	2.91±0.03	107±12
ST4	39.2±1.2	136±1	1708±30	480±60	17.3±0.1	121.8±0.2	2.91±0.03	103±11
ST6	37.1±1.2	162±1	1356±28	463±50	18.5±0.1	97.7±0.2	3.40±0.03	92±10
ST7	38.8±1.2	163±1	1205±26	351±43	19.9±0.1	92.9±0.2	3.61±0.03	100±11
ST8	40.0±1.2	159±1	1382±28	365±45	19.4±0.1	98.5±0.2	3.56±0.03	91±11
ST9-12	25.8±1.0	161±1	3050±38	964±64	15.3±0.1	85.0±0.2	2.67±0.02	85±9
Sediment traps, 1000 m-depth.								
ST2	41.4±1.7	147±1	1034±32	212±48	20.8±0.2	97.4±0.3	3.36±0.04	106±14
ST3	34.4±.7	134±1	1529±43	268±72	17.6±0.2	116.3±0.3	2.99±0.04	90±16
ST4	39.7±.6	134±1	1508±38	413±76	17.5±0.1	119.0±0.3	3.04±0.03	114±14
ST5	30.5±1.2	145±1	1581±34	372±65	16.1±0.1	120.4±0.3	2.73±0.03	86±12
ST6	36.0±1.3	156±1	1148±28	342±44	18.9±0.1	93.9±0.2	3.48±0.03	95±11
ST7	40.1±1.2	156±	1064±25	312±40	20.0±0.1	94.1±0.2	3.65±0.03	96±11
ST8	39.9±1.2	156±	1221±26	385±48	1.92	101.0±0.2	3.47±0.03	84±10
ST9	37.0±1.5	166±1	1915±37	417±61	18.5±0.1	97.4±0.2	2.84±0.03	83±10
ST10	33.2±1.1	158±1	1493±29	311±48	16.9±0.1	108.3±0.2	2.98±0.03	103±11
ST11	30.0±1.1	165±1	2084±34	406±52	16.0±0.1	95.5±0.2	2.77±0.03	84±10
ST12	21.8±0.9	172±1	3770±43	389±51	13.1±0.1	82.0±0.2	2.14±0.03	72±9

Table i.b. Trace element composition of samples determined by X-ray Fluorescence (XRF; n= 1). Uncertainties provided for k = 1 (65.3% confidence interval).

Element	Cr	Mn	Fe	Ni	Cu	Zn	Ga	As
Sample	µg/g	µg/g	mg/g	µg/g	µg/g	µg/g	µg/g	µg/g
Atmospheric dust.								
SD1	211±7	589±9	40.9±0.2	73±2	116±2	246±2	17.6±0.6	8.6±0.8
SD2	654±11	556±9	42.8±0.2	201±3	568±4	662±4	15.9±0.6	10.8±1.0
Sediment traps, 200 m-depth.								
ST2	96±6	808±12	35.6±0.1	60±2	45±1	137±2	18.8±0.8	18.3±1.0
ST3	95±6	1085±13	32.2±0.1	57±2	39±1	179±2	16.7±0.8	16.8±1.0
ST4	95±7	1198±15	33.3±0.1	66±2	41±2	188±2	14.6±0.7	18.1±1.1
ST6	63±5	614±10	32.9±0.1	45±2	29±1	113±2	14.9±0.7	11.4±0.8
ST7	60±5	580±10	35.2±0.1	41±2	30±1	108±2	16.4±0.7	10.8±0.8
ST8	60±5	565±10	34.6±0.1	42±2	31±1	137±2	14.4±0.7	11.9±0.8
ST9-12	57±5	413±8	28.6±0.1	40±2	31±1	165±2	13.2±0.6	10±0.7
Sediment traps, 1000 m-depth.								
ST2	110±7	990±14	35.4±0.1	68±2	44±2	132±2	17.9±0.9	15.9±1.1
ST3	99±8	1267±17	34.1±0.1	68±3	41±2	129±2	14.1±0.8	19.5±1.2
ST4	87±7	1257±15	34.3±0.1	63±2	46±2	133±2	14.2±0.8	19.9±1.1
ST5	99±7	930±13	31.3±0.1	68±2	43±2	133±2	13.1±0.7	15.7±1.0
ST6	56±5	642±10	34.3±0.1	45±2	36±1	97±2	16.1±0.7	10.1±0.8
ST7	48±4	600±10	35.4±0.1	41±2	37±1	92±2	17.7±0.7	10.4±0.8
ST8	68±5	680±10	34.9±0.1	52±2	44±1	109±2	15.9±0.4	12.6±0.8
ST9	64±5	631±10	29.8±0.1	46±2	41±1	108±2	13.5±0.6	10.1±0.8
ST10	61±5	722±11	31.3±0.1	49±2	47±1	126±2	14.0±0.6	12.7±0.8
ST11	74±6	690±10	29.6±0.1	57±2	50±1	127±2	13.3±0.7	13.8±0.8
ST12	50±5	523±9	23.5±0.1	48±2	48±1	134±2	10.9±0.6	10.0±0.8

Table i.3. Trace element composition of samples determined by X-ray Fluorescence (XRF; n= 1). Uncertainties provided for k = 1 (65.3% confidence interval).

Element	Br	Rb	Sr	Y	Zr	Nb	Sn
Sample	µg/g	µg/g	µg/g	µg/g	µg/g	µg/g	µg/g
Atmospheric dust.							
SD1	7.5±0.3	86±1	212±1	25.1±0.5	193±5	10.9±1.6	7.0±0.4
SD2	10.0±0.3	82±1	148±1	25.1±0.5	182±5	9.0±1.6	15.9±0.5
Sediment traps, 200 m-depth.							
ST2	89±1	130±1	560±2	18.4±0.6	107±5	5.5±1.4	4.7±0.4
ST3	199±1	111±1	824±2	14.0±0.5	87±5	6.2±1.4	2.4±0.3
ST4	228±1	107±1	932±2	14.6±0.6	87±6	4.9±1.4	2.9±0.4
ST6	149±1	84±1	527±1	17.8±0.5	135±5	8.4±1.4	1.1±0.2
ST7	107±1	85±1	447±1	20.6±0.5	142±5	9.3±1.4	0.8±0.2
ST8	130±1	85±1	490±1	19.5±0.5	136±5	7.1±1.4	1.8±0.3
ST9-12	554±2	72±1	470±	12.3±0.4	79±4	5.1±1.2	2.7±0.3
Sediment traps, 1000 m-depth.							
ST2	140±1	129±1	640±2	18.3±0.6	106±5	8.3±1.4	8.9±0.5
ST3	218±1	110±1	864±2	15.8±0.6	76±5	8.7±1.4	5.4±0.4
ST4	205±1	110±1	892±2	14.6±0.6	72±6	9.0±1.5	4.9±0.5
ST5	232±1	98±1	894±2	13.9±0.6	80±6	7.6±1.4	4.1±0.4
ST6	125±1	85±1	466±1	19.6±0.5	157±5	11.0±1.5	2.9±0.3
ST7	97±1	86±1	433±1	20.9±0.5	152±5	8.9±1.4	1.8±0.3
ST8	129±1	89±1	527±1	18.3±0.5	120±5	7.5±1.4	2.1±0.3
ST9	172±1	78±	493±1	15.0±0.4	76±5	4.1±1.4	0.5±0.1
ST10	195±1	83±1	605±2	16.0±0.5	101±5	6.0±1.3	1.9±0.3
ST11	424±2	81±1	525±1	13.3±0.5	91±4	6.5±1.3	2.3±0.3
ST12	1311±3	69±	472±1	9.2±0.4	61±4	4.0±1.1	1.9±0.3

Table i.d. Trace element composition of samples determined by X-ray Fluorescence (XRF; n= 1). Uncertainties provided for k = 1 (65.3% confidence interval).

Element	I	Ba	La	Ce	Pb	Th	U
Sample	µg/g	µg/g	µg/g	µg/g	µg/g	µg/g	µg/g
Atmospheric dust.							
SD1	3.7±1.0	392±3	24.1±3.2	49.2±4.2	52±1	8.6±0.5	2.03±0.02
SD2	3.3±1.0	365±3	18.7±3.1	45.9±4.0	95±1	5.9±0.3	2.04±0.02
Sediment traps, 200 m-depth.							
ST2	49±1	297±3	18.9±3.1	48.1±4.0	52±1	9.9±0.6	N.M.
ST3	90±2	478±4	21±4	56.0±5.2	58±1	9.5±0.6	1.77±0.02
ST4	110±2	630±5	28.5±4.9	55.8±6.4	61±1	9.9±0.6	N.M.
ST6	56±1	360±3	14.8±2.9	33.7±3.7	34±1	7.8±0.5	1.65±0.02
ST7	69±1	367±3	25.4±3.0	39.7±3.8	33±1	7.6±0.5	1.72±0.02
ST8	116±2	448±4	24.8±3.8	48.9±4.9	32±1	8.6±0.6	1.78±0.02
ST9-12	141±2	321±3	< 4.9	14.1±3.1	32±1	7.6±0.6	1.48±0.02
Sediment traps, 1000 m-depth.							
ST2	102±2	457±4	31.1±4.1	61.2±5.4	59±1	12.4±0.7	N.M.
ST3	97±2	581±5	26.1±4.2	48.2±5.4	59±1	11.1±0.7	1.79±0.02
ST4	115±2	725±6	36.6±5.9	65.2±7.6	58±1	11.9±0.7	N.M.
ST5	104±2	662±5	32.8±4.8	44±6	50±1	9.7±0.6	N.M.
ST6	44±1	384±3	20.2±3.0	44.1±3.9	36±1	7.9±0.6	1.70±0.02
ST7	39±1	378±3	20.2±3.1	40.6±3.9	34±1	8.0±0.5	1.60±0.02
ST8	61±1	419±3	18.5±3.0	36.2±3.8	39±1	9.0±0.5	1.73±0.02
ST9	56±1	347±3	16.5±3.1	15.4±3.5	38±1	6.6±0.5	1.75±0.02
ST10	79±2	536±4	13.4±3.4	22.3±4.4	41±1	7.2±0.5	N.M.
ST11	70±2	437±4	10.4±3.0	31.9±4.3	40±1	8.8±0.6	N.M.
ST12	73±1	425±4	13.6±3.1	23.9±3.9	36±1	8.4±0.7	N.M.

Table ii.a: Element vertical fluxes.

Mass flux / Sample	Al (mg/m^2·d)	Si (mg/m^2·d)	S (μg/m^2·d)	P (μg/m^2·d)	K (mg/m^2·d)	Ca (mg/m^2·d)	Ti (mg/m^2·d)	V (μg/m^2·d)
200 m-depth								
ST-2	27.25 ±0.82	91.81±0.58	601±15	132±22	12.632±0.058	58.19±0.12	2.035±0.018	64.9±6.4
ST-3	7.10 ±0.25	24.26±0.18	304.1±6.0	81±12	3.147±0.018	21.096±0.035	0.5116±0.0053	18.8±2.1
ST-4	5.13 ±0.16	17.80±0.13	223.6±3.9	62.8±7.8	2.265±0.013	15.944±0.026	0.3809±0.0039	13.5±1.4
ST-6	45.6 ±1.5	198.9±1.2	1665±34	569. ±61	22.72±0.12	119.98±0.25	4.175±0.037	113±12
ST-7	33.1 ±1.0	138.99±0.85	1027±22	299±37	16.969±0.085	79.22±0.17	3.078±0.025	85.3±9.4
ST-8	9.36 ±0.28	37.22±0.23	323.5±6.6	85±10	4.541±0.023	23.059±0.047	0.8334±0.0070	21.3±2.6
ST-9-12	5.39 ±0.21	33.66±0.20	637.8±7.9	202±13	3.199±0.021	17.774±0.042	0.5583±0.0042	17.8±1.9
1000 m-depth								
ST-2	6.47 ±0.27	22.98±0.16	161.6±5.2	33.1±7.5	3.254±0.032	15.224±0.047	0.5253±0.0064	16.6±2.2
ST-3	4.84 ±0.10	18.84±0.14	215±6.0	38±10	2.473±0.032	16.352±0.042	0.4220±0.0064	12.7±2.2
ST-4	3.39 ±0.05	11.43±0.09	128.6±3.2	35.2±6.5	1.493±0.011	10.151±0.026	0.2593±0.0034	9.7±1.2
ST-5	3.5 ±0.14	16.66±0.11	181.7±3.9	42.7±7.5	1.851±0.014	13.834±0.034	0.3142±0.0031	9.9±1.4
ST-6	26.05 ±0.94	112.9±0.72	831±20	247.5±32	13.68±0.074	67.96±0.14	2.518±0.022	68.8±8
ST-7	35.8 ±1.1	139.37±0.28	951±22	287±36	17.872±0.094	84.07±0.18	3.261±0.027	85.8±9.8
ST-8	22.29 ±0.67	87.16±0.33	682±14	215±27	1.075±0.069	56.43±0.11	1.939±0.017	46.9±5.6
ST-9	20.9 ±0.85	93.77±0.56	1081.8±21	236±34	10.452±0.063	55.02±0.11	1.604±0.017	46.9±5.6
ST-10	5.74 ±0.19	27.33±0.17	258.3±5.2	53.8±8.3	2.921±0.023	18.736±0.035	0.5164±0.0053	17.8±1.9
ST-11	7.31 ±0.27	40.23±0.24	508.1±8.3	99±13	3.900±0.028	23.283±0.049	0.6754±0.0071	20.5±2.4
ST-12	5.41 ±0.22	42.67±0.25	935±11	96.5±13	3.251±0.023	20.344±0.050	0.5312±0.0072	17.9±2.2

Table ii.b. Element vertical fluxes (Cont'd).

Mass flux / Sample	Cr (μg/m²·d)	Mn (μg/m²·d)	Fe (mg/m²·d)	Ni (μg/m²·d)	Cu (μg/m²·d)	Zn (μg/m²·d)	Ga (μg/m²·d)	As (μg/m²·d)
200 m-depth								
ST-2	56.1±3.5	472.5±7.0	20.819±0.058	35.1±1.2	26.32±0.58	80.1±1.2	10.99±0.47	10.7±0.58
ST-3	16.7±1.1	190.7±2.3	5.661±0.018	10.02±0.35	6.86±0.18	31.47±0.35	2.94±0.14	2.95±0.18
ST-4	12.4±0.9	156.8±2.0	4.359±0.013	8.64±0.26	5.37±0.26	24.61±0.26	1.911±0.092	2.37±0.14
ST-6	77.4±6.1	754±12	40.40±0.12	55.3±2.5	35.61±1.23	138.8±2.5	18.297±0.86	14±0.98
ST-7	51.2±4.3	494.6±8.5	30.015±0.085	35.0±1.7	25.58±0.85	92.1±1.7	13.98±0.60	9.21±0.68
ST-8	14±1.2	132.3±2.3	8.100±0.023	9.83±0.47	7.26±0.23	32.07±0.47	3.37±0.16	2.79±0.19
ST-9-12	11.9±1	86.4±1.7	5.980±0.021	8.36±0.42	6.48±0.21	34.50±0.42	2.76±0.12	2.09±0.15
1000 m-depth								
ST-2	17.2±1.1	154.7±2.2	5.533±0.016	10.63±0.31	6.88±0.31	20.63±0.31	2.80±0.14	2.49±0.17
ST-3	13.9±1.1	178.1±2.4	4.794±0.014	9.56±0.42	5.76±0.28	18.14±0.28	1.98±0.11	2.74±0.17
ST-4	7.42±0.60	107.2±1.3	2.926±0.009	5.37±0.17	3.92±0.17	11.34±0.17	1.212±0.073	1.720±0.092
ST-5	11.4±0.8	106.9±1.5	3.596±0.011	7.81±0.23	4.94±0.23	15.28±0.23	1.512±0.084	1.8±0.11
ST-6	40.5±3.6	464.6±7.2	24.823±0.072	32.6±1.4	26.05±0.72	70.2±1.4	11.65±0.51	7.31±0.58
ST-7	42.9±3.6	536±8.9	31.626±0.089	36.6±1.8	33.06±0.89	82.2±1.8	15.81±0.63	9.29±0.71
ST-8	38±2.8	379.9±5.6	19.499±0.056	29.0±1.1	24.58±0.56	60.9±1.1	8.88±0.22	7.04±0.45
ST-9	36.2±2.8	356.5±5.6	16.834±0.056	26.0±1.1	23.16±0.56	61.0±1.1	7.63±0.34	5.71±0.45
ST-10	10.6±0.9	124.9±1.9	5.415±0.017	8.48±0.35	8.13±0.17	21.8±0.35	2.42±0.10	2.23±0.14
ST-11	18±1.5	168.2±2.4	7.216±0.024	13.91±0.49	12.19±0.24	30.96±0.49	3.24±0.17	3.36±0.23
ST-12	12.4±1.2	129.8±2.2	5.83±0.025	11.91±0.50	11.91±0.25	33.25±0.50	2.70±0.15	2.48±0.23

Table ii.c. Element vertical fluxes (Cont'd).

Mass flux / Sample	Br (μg/m²·d)	Rb (μg/m²·d)	Sr (μg/m²·d)	Y (μg/m²·d)	Zr (μg/m²·d)	Nb (μg/m²·d)	Sn (μg/m²·d)
200 m-depth							
ST-2	52.05±0.58	76.02±0.58	327.5±1.2	10.76±0.35	62.6±3.0	3.22±0.82	2.75±0.23
ST-3	34.98±0.18	19.51±0.18	144.86±0.35	2.464±0.093	15.29±0.88	1.09±0.25	0.423±0.052
ST-4	29.85±0.13	14.01±0.13	122.04±0.26	1.912±0.084	11.39±0.79	0.64±0.18	0.384±0.054
ST-6	183.0±1.2	103.2±1.2	647.2±1.2	21.86±0.61	165.8±6.1	10.3±1.7	1.35±0.25
ST-7	91.24±0.85	72.48±0.85	381.16±0.85	17.57±0.43	121.1±4.3	7.9±1.2	0.68±0.17
ST-8	30.43±0.23	19.90±0.23	114.71±0.23	4.56±0.12	31.8±1.2	1.66±0.33	0.420±0.073
ST-9-12	115.84±0.42	15.06±0.21	98.28±0.39	2.572±0.085	16.52±0.84	1.07±0.25	0.560±0.062
1000 m-depth							
ST-2	21.88±0.16	20.16±0.16	100.03±0.31	2.863±0.093	16.57±0.78	1.30±0.22	1.393±0.082
ST-3	30.65±0.14	15.47±0.14	121.48±0.28	2.221±0.084	10.69±0.70	1.22±0.20	0.761±0.064
ST-4	17.494±0.094	9.383±0.092	76.09±0.17	1.252±0.054	6.14±0.51	0.77±0.13	0.423±0.043
ST-5	26.66±0.11	11.26±0.11	102.72±0.23	1.621±0.072	9.19±0.69	0.87±0.16	0.470±0.052
ST-6	90.46±0.72	61.51±0.72	337.24±0.72	14.18±0.36	113.6±3.6	7.96±1.09	2.10±0.22
ST-7	86.66±0.89	76.83±0.89	386.84±0.89	18.67±0.45	135.8±4.5	8.0±1.3	1.61±0.27
ST-8	72.07±0.56	49.72±0.56	294.43±0.56	10.22±0.28	67.0±2.8	4.19±0.78	1.17±0.17
ST-9	97.16±0.56	44.06±0.62	278.53±0.56	8.47±0.23	42.9±2.8	2.32±0.79	0.282±0.062
ST-10	33.74±0.17	14.36±0.17	104.67±0.35	2.774±0.091	17.47±0.87	1.04±0.22	0.330±0.054
ST-11	103.37±0.49	19.75±0.24	128.08±0.24	3.24±0.12	22.19±0.98	1.58±0.32	0.561±0.072
ST-12	325.26±0.74	17.12±0.25	117.10±0.25	2.28±0.14	15.13±0.99	0.99±0.27	0.472±0.073

Table ii.d. Element vertical fluxes (Cont'd).

Mass flux / Sample	I (μg/m²·d)	Ba (μg/m²·d)	La (μg/m²·d)	Ce (μg/m²·d)	Pb (μg/m²·d)	Th (μg/m²·d)	U (μg/m²·d)
200 m-depth							
ST-2	28.66±0.58	173.7±1.8	11.0±1.8	28.1±2.3	30.41 ±0.58	5.79 ±0.35	N.M.
ST-3	15.82±0.35	84.03±0.70	3.69±0.70	9.84±0.91	10.20±0.18	1.67 ±0.10	0.3114 ±0.0028
ST-4	14.4±0.26	82.47±0.65	3.73±0.64	7.33±0.84	7.98 ±0.13	1.296 ±0.078	N.M.
ST-6	68.8±1.2	442.1±3.7	18.2±3.6	41.4±4.5	41.8 ±7.2	9.58 ±0.61	2.024 ±0.099
ST-7	58.84±0.85	313.0±2.6	21.7±2.6	33.8±3.2	28.14 ±0.85	6.48 ±0.43	1.467 ±0.014
ST-8	27.16±0.47	104.88±0.94	5.81±0.89	11.4±1.2	7.49 ±0.23	2.01 ±0.14	0.4178 ±0.0038
ST-9-12	29.48±0.42	67.12±0.63	-	2.95±0.65	6.69 ±0.21	1.59 ±0.12	0.3093 ±0.0017
1000 m-depth							
ST-2	15.94±0.31	71.41±0.65	4.86±0.64	9.57±0.84	9.22 ±0.16	1.94 ±0.11	N.M.
ST-3	13.64±0.28	81.73±0.73	3.67±0.59	6.78±0.76	8.30 ±0.14	1.561 ±0.098	0.2521 ±0.0023
ST-4	9.81±0.17	61.83±0.54	3.12±0.50	5.56±0.65	4.947 ±0.085	1.015 ±0.060	N.M.
ST-5	11.95±0.23	76.10±0.62	3.77±0.55	5.06±0.69	5.74 ±0.12	1.114 ±0.069	N.M.
ST-6	31.84±0.72	277.9±2.2	14.6±2.2	31.9±2.8	26.05 ±0.72	5.71 ±0.43	1.2335 ±0.0058
ST-7	34.84±0.89	337.7±2.7	18±2.8	36.3±3.5	30.38 ±0.89	7.15 ±0.45	1.429 ±0.014
ST-8	34.08±0.56	234.1±1.7	10.3±1.7	20.2±2.1	21.79 ±0.56	5.028 ±0.28	0.9658 ±0.0090
ST-9	31.63±0.56	196.1±1.7	9.3±1.8	8.7±2.0	21.47 ±0.56	3.73 ±0.28	0.9901 ±0.0091
ST-10	13.67±0.35	92.72±0.70	2.32±0.59	3.86±0.76	7.09 ±0.17	1.246 ±0.086	N.M.
ST-11	17.07±0.49	106.5±1.0	2.54±0.73	7. 8±1.0	9.75 ±0.24	2.14 ±0.15	N.M.
ST-12	18.11±0.25	105.4±1.0	3.37±0.77	5.9±1.0	8.93 ±0.25	2.08 ±0.17	N.M.